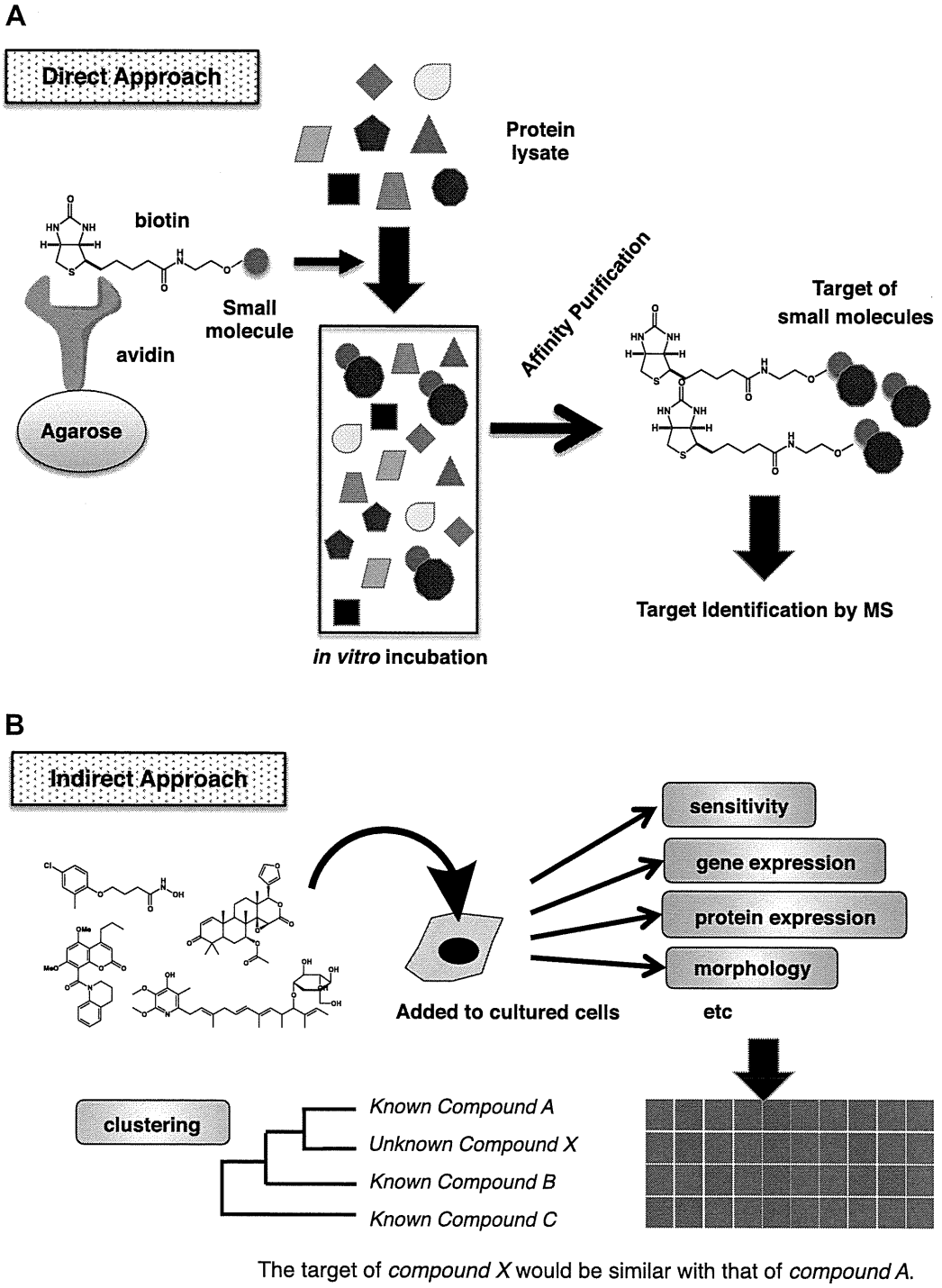


**Figure 1.** Schematic illustration of 'Direct Approach' and 'Indirect Approach'. (A) The strategy of target identification by using biotin-affinity tags is shown. Cell lysates are incubated with biotin-tagged small molecules and the binding-protein is purified with avidin-agarose before identification using mass spectrometry (MS). (B) The strategy of target identification by profiling is shown. Target-known and target-unknown small molecules are added to cultured cells and the cellular responses, such as drug sensitivity, gene expression, protein expression, or morphological changes, are collected. The profiling from the collected data predicts the target of the small molecule of interest.

small molecules. In particular, affinity chromatography using a biotin affinity tag or Affi-gel system has been successful, but is disadvantaged by the fact that small molecules can lose their biological activity due to the presence of the biotin affinity tag or Affi-gel tag at the active site. To overcome this issue, new methods such as click chemistry, photo-crosslink, and FG beads are now in development. This section highlights recent successes using affinity chromatography as the 'Direct approach'.

### 2.1. Biotin affinity tag

Target identification using a biotin-affinity tag was first developed by Professor Stuart L. Schreiber.[12] At present, this method was believed to be a powerful tool to identify target proteins. Indeed, many target proteins have since been identified using this method, including target proteins of chromeceptin,[13] withaferin A,[14] tetrahydroisoquinoline,[15] spliceostatin,[16] pladienolide,[17] and

fatostatin[18] (Fig. 2). Chromeceptin was identified as an inhibitor for insulin-induced adipogenesis,[19] and was suggested to exert its biological activity by blocking the autocrine loop of IGF2. Furthermore, chromeceptin activates the transcription factor STAT6, resulting in up-regulation of IGFBP-1 (IGF binding protein 1) and SOCS-3 (suppressor of cytokine signaling 3). IGFBP-1 is known to be a secreted IGF-binding polypeptide which inhibits IGF2. On the other hand, SOCS-3 is reported to suppress insulin-induced tyrosine phosphorylation of insulin receptor substrate (IRS-1), causing insulin resistance. Therefore, chromeceptin was suggested to inhibit insulin-induced adipogenesis through STAT6-stimulated IGFBP-1 and SOCS-3 up-regulation. However, its precise mechanism of action was unknown. Uesugi and co-workers identified MFP-2 (multifunctional protein 2), which is involved in the peroxisomal β-oxidation of fatty acids, as a chromeceptin-binding protein by affinity purification using biotinylated-chromeceptin.[13] Knockdown of MFP-2 suppressed chromeceptin-increased IGFBP-1 expression. These results collectively suggest that MFP-2 is essential for chromeceptin-induced STAT6 activation. Their study provided chemical genetic support for the role of the STAT-SOCS pathway in IGF regulation, and implicated a new pathway for STAT6 activation.

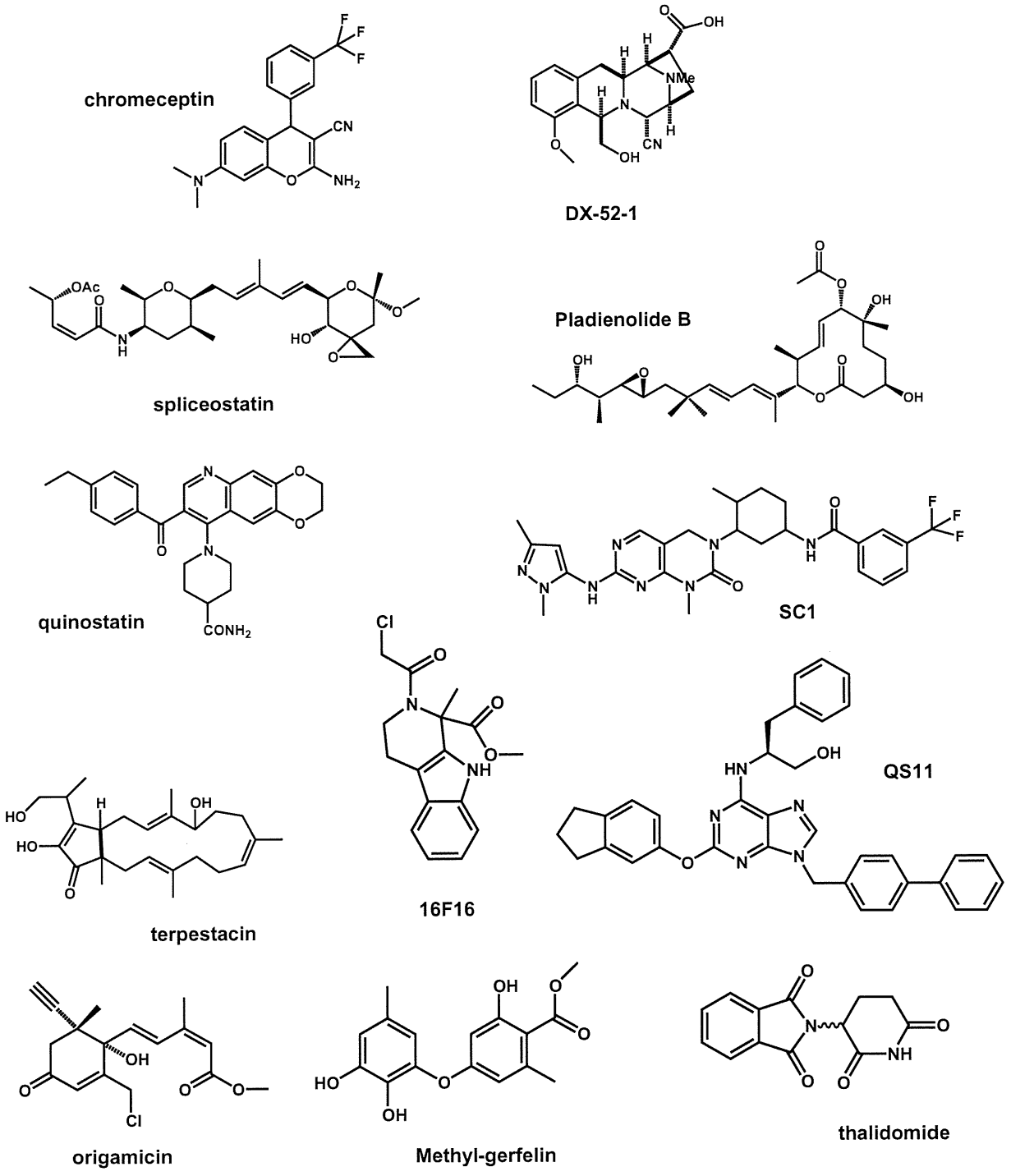


**Figure 2.** Structure of small molecules whose targets were identified by the 'Direct Approach'.

**Table 1**
Summary of small molecules whose targets were identified by the 'Direct Approach' or the 'Indirect Approach'

| Method category | | Compound name | Original bioactivity | Target protein | Journal | First author | Year |
|---|---|---|---|---|---|---|---|
| Direct approach | Biotin-affinity tag | Chromeceptin | Anti-adipogenesis | MFP-2 | Chem. Biol. | Yongmun Choi | 2006 |
| | | Withaferin A | Anti-cell migration | Annexin-II | Nat. Chem. Biol | Ryan R. Falsey | 2006 |
| | | DX-52-1 | Anti-cell migration | Radixin | Chem. Biol. | Alem W. Kahsai | 2006 |
| | | DX-52-1 | Anti-cell migration | Galectin-3 | J. Biol. Chem. | Alem W. Kahsai | 2008 |
| | | Spliceostatin | Anti-tumor | SF3b | Nat. Chem. Biol. | Daisuke Kaida | 2007 |
| | | Pladienolide | Anti-tumor | SF3b | Nat. Chem. Biol. | Yoshihiko Kotake | 2007 |
| | | Fatostatin | Anti-adipogenesis | SCAP | Chem. Biol. | Shinji Kamisuki | 2009 |
| | Affi-Gel tag | SC1 | Regulation of self-differentiation of ES cells | RasGAP/ERK1 | PNAS | Shinji Kamisuki | 2009 |
| | | Quinostatin | mTOR inhibitor | PI3K p110 | Chem. Biol. | Jiong Yang | 2007 |
| | | QS11 | TCF transcriptional activation | ARFGAP1 | PNAS | Qisheng Zhang | 2007 |
| | Phage display | Terpestacin | Anti-angiogenic | UQCRB (mitochondrial complex III) | J. Biol. Chem. | Hye Jin Jung | 2010 |
| | Click chemistry | Origamicin | Anti-HCV activity | PDI | Chem. Biol. | Bojana Rakic | 2006 |
| | | 16F16 | Anti-huntingtin | PDI | Nat. Chem. Biol. | Benjamin G. Hoffstrom | 2010 |
| | Photo-crosslink | Methyl-gerfelin | Anti-cell migration | Glyoxalase I | PNAS | Makoto Kawatani | 2008 |
| | FG-beads | Thalidomide | Teratogenicity | Cereblon | Science | Takumi Ito | 2010 |
| Indirect approach | DARTS | Resveratrol | Antioxidant | eIF4A | PNAS | Brett Lomenick | 2009 |
| | COMPARE analysis | ZSTK474 | Kinase inhibitor | PI3K | J. Netl. Can. Inst. | Shin-ichi Yaguchi | 2006 |
| | Connectivity Map | Gedunin | Anti-malarial activity | HSP90 | Cancer Cell | Haley Hieronymus | 2006 |
| | | Celasteol | Growth inhibition | HSP90 | Cancer Cell | Haley Hieronymus | 2006 |
| | | Droxinostat | Enhancing CH-11-induced apoptosis | HDAC | Mol. Cancer Ther. | Tabitha E. Wood | 2010 |
| | Proteomic profiling | BNS-22 | Growth inhibition | Topoisomerase II | Chem. Biol. | Makoto Kawatani | 2011 |
| | Morphological profiling | Pseudolarix acid B | Anti-fungal activity | Microtubule | Nat. Chem. Biol. | Daniel W. Young | 2008 |
| | | Bisebromoamide | Cytotoxicity | Actin | ACS Chem. Biol. | Eriko Sumiya | 2011 |
| | | Miuraenamide A | Anti-fungal activity | Actin | ACS Chem. Biol. | Eriko Sumiya | 2011 |
| | Metabolomic profiling | Glucopiericidin A | Filopodia inhibition | Glucotransporter | Chem. Biol. | Mitsuhiro Kitagawa | 2010 |
| | Chemical-genetic profiling | Papuamide B | Anti-HIV activity | Phosphatidylserine | Cell | Ainslie B. Parsons | 2006 |
| | | Leucascandrolide | Cell growth inhibition | Cytcrome bc1 complex | Nat. Chem. Biol. | Olesya A. Ulanovskaya | 2008 |
| | | Theonellamide F | Anti-fungal activity | 3β-Hydroxysterols | Nat. Chem. Biol. | Shinichi Nishimura | 2010 |

Tetrahydroisoquinoline DX-52-1, a semi-synthetic derivative of quinocarmycin, was identified as an inhibitor of cell migration.[20] By using biotinylated-DX-52-1, Fenteany and co-workers reported that radixin was the primary target of DX-52-1.[20] Radixin is a member of the ezrin/radixin/moesin (ERM) family of membrane-actin cytoskeleton linker proteins,[21] and ERM family proteins have been reported to bind to actin and various cell adhesion molecules, such as CD44. To elucidate the involvement of radixin in DX-52-1-inhibited cell migration, the authors investigated the effects of DX-52-1 on cell migration in radixin-overexpressing or radixin-knockdown cells. Overexpression of radixin made cells less sensitive to the anti-migratory activity of DX-52-1, whereas radixin knockdown using siRNA resulted in a reduced rate of cell migration, suggesting that radixin plays an important role in DX-52-1-inhibited cell migration. To further address the biological function of radixin in DX-52-1-inhibited cell migration, the authors examined the interaction between radixin and actin or CD44. They found that DX-52-1 disrupted radixin's ability to interact with both actin and CD44, which resulted in an inhibition of cell migration. On the other hand, although radixin was the most intensely labeled protein by biotinylated-DX-52-1, three other less intensely labeled proteins were also detected. Further research aimed at identifying these other proteins found that galectin-3, a family of lectins, was a secondary target of DX-52-1.[15] Similar to radixin, overexpression of galectin-3 decreased sensitivity to the anti-migratory activity of DX-52-1, whereas knockdown of galectin-3 resulted in decreased cell motility and cell adhesion. These results also suggested that galectin-3 plays an important role in DX-52-1-inhibited cell migration. However, the functional correlation between radixin and galectin-3 in cell motility and cell adhesion remains unclear.

The natural product FR901464 was isolated from a fermentation broth of the bacterium *Pseudomonas* sp. as an anti-cancer compound that enhances the transcriptional activity of the SV40 promoter, causes cell cycle arrest at the G1 and G2/M phases,[22,23] and induces abnormal mRNA splicing. However, the molecular mechanism of FR901464 was unknown. Yoshida et al. performed a SAR study to identify which moiety of FR901464 could be attached to biotin, without losing its biological activity. They succeeded in synthesizing a more potent methyl ketal derivative of FR901464, named spliceostatin, and also in synthesizing biotinylated-spliceostatin. By using biotinylated-spliceostatin, they were able to identify the SF3b complex, a subcomplex of the U2 small nuclear ribonucleoprotein (snRNP) in the spliceosome, as a target of spliceostatin. As SF3b has an important role in the U2 snRNP, which binds to the mRNA branchpoint sequence, spliceostatin

was shown to inhibit in vitro and in vivo splicing and promote pre-mRNA (unspliced mRNA) accumulation by binding to SF3b. Furthermore, spliceostatin leaks pre-mRNA into the cytosol, where it is translated. This study showed that the inhibition of pre-mRNA splicing during early steps involving SF3b allows unspliced mRNA leakage and translation.[16] Interestingly, SF3b was also identified as a target of pladienolide by Mizui et al.[17] Pladienolide was isolated from the fermentation broth of *Streptomyces platensis* Mer-11107 as an anti-tumor macrolide, which was discovered by using a cell-based reporter gene expression assay controlled by the human vascular endothelial growth factor promoter.[24–26] They first synthesized fluorescence-tagged pladienolide to monitor the intracellular localization of the target protein. HeLa cells treated with fluorescence-tagged pladienolide showed localization of the pladienolide to the granular structure in the nuclei. These granules overlapped with the localization of splicing factor SF3b. Furthermore, SF3b was confirmed to be a target of pladienolide by purification of the binding protein using biotinylated-pladienolide. Like spliceostatin, pladienolide also inhibited in vivo splicing. These two small molecules showed anti-tumor activity, and these studies suggest that the SF3b complex is a potential anti-tumor drug target. Indeed, pladienolide is now in phase I clinical trials.

### 2.2. Affi-Gel tag

As well as the biotin affinity tag, purification of the target protein using Affi-gel is also an excellent strategy. The Affi-gel matrix is able to directly link to the small molecule of interest. Thus, compared with the biotin-affinity tag, the number of non-specific interactions with the affinity matrix is reduced. Here, we highlight target proteins of several bioactive small molecules which were identified by using the Affi-gel system. Embryonic stem cells (ES cells) provide an excellent in vitro system for the study of early development and human disease. However, the mechanisms that govern their self-renewal and differentiation are largely unknown. Thus, small molecules that maintain self-renewal or promote differentiation would be useful discoveries to understand self-renewal and differentiation mechanisms. SC1, a derivative of 3,4-dihydropyrimido[4,5-*d*]pyrimidine, was identified to maintain the undifferentiated phenotype of mouse ES (mES) cells by Ding et al.[27] To identify the cellular target of SC1, SC1 was linked at the N1 position to an agarose affinity matrix via a polyethylene glycol linker. Whole-cell lysates of mES cells were incubated with this affinity matrix and the binding proteins were purified and analyzed by liquid chromatography–mass spectrometry (LC/MS). As a result, the SC1-binding proteins were identified as ERK1 and RasGAP. Direct binding of SC1 to ERK1 or RasGAP was confirmed by surface plasmon resonance (SPR). Further biochemical and cellular experiments suggested that SC1 works through dual inhibition of ERK1 and RasGAP.

The mammalian target of the rapamycin (mTOR) signaling network is crucial for the regulation of cell growth in response to both growth factors and nutrients. Although carbon and nitrogen sources, such as glucose and glutamine, are primary stimuli of mTOR, the mechanism by which they stimulate the mTOR pathway are still unknown. Thus, Schreiber and co-workers screened small molecule modulators of mTOR signaling.[28] From a collection of ~20,000 compounds in the library, they discovered quinostatin as an inhibitor of mTOR signaling. Since the molecular target of quinostatin was unknown, they carried out affinity chromatography purification to identify this target protein. An analog of quinostatin was prepared by attaching a polyethylene glycol linker, and this polyethylene glycol-modified quinostatin was immobilized to agarose beads. To isolate the target protein of quinostatin, MCF7 cell lysates were incubated with the affinity reagent. After LC/MS analysis, the target protein of quinostatin was found to be the catalytic subunit of the class Ia PI3Ks.

Similarly, QS11, a purine derivative, that synergizes with a Wnt-3a ligand in the activation of Wnt/β-catenin signal transduction, was shown to bind the GTPase activating protein of ADP-ribosylation factor 1 (ARFGAP1) by using the Affi-Gel system. ARFGAPs form a family of GTPase-activating proteins that regulate the small GTPase ADP-ribosylation factors (ARFs). ARFGAPs promote ARF inactivation by stimulating GTP hydrolysis, whereas guanine nucleotide exchange factors of ARF (ARFGEFs) catalyze the formation of active GTP-bound ARFs. QS11 significantly increased the levels of GTP-bound ARFs in NIH3T3 cells, suggesting that QS11 inhibited ARFGAPs. It has been reported that the activation of ARFs promotes the dissociation of membrane-bound β-catenin.[29] Thus, QS11 was suggested to inhibit ARFGAP, thereby leading to an increase in activated ARF and subsequent β-catenin translocation. The released β-catenin accumulates and translocates to the nucleus when cells are stimulated with Wnt-3a.

### 2.3. Phage display

Terpestacin was identified to inhibit the functional response to hypoxia of human umbilical vein endothelial cells in vitro and angiogenesis within the embryonic chick chorioallantonic membrane in vivo.[30] Furthermore, terpestacin has been shown to inhibit hypoxia-induced HIF-1α and VEGF expression. These results indicate that terpestacin inhibits hypoxia-induced tumor angiogenesis via the inhibition of HIF-1α-mediated VEGF expression. To better understand the cellular mechanisms of its anti-angiogenic activity, Kwon et al. aimed to identify the target molecule for terpestacin by using phage display biopanning.[31] They first synthesized biotinylated-terpestacin, which was then immobilized on a streptavidin-coated well plate, and four rounds of phage biopanning were conducted using T7 phages expressing functional human cDNA libraries. As a result, UQCRB, a 13.4 kDa subunit of complex III in the mitochondrial respiratory chain,[32] was identified as a terpestacin-binding protein. Knockdown of UQCRB by siRNA resulted in inhibition of hypoxia-induced HIF-1α accumulation and VEGF expression in HT1080 cells. These results suggest that UQCRB plays a key role in the cellular oxygen-sensing and transduction systems. This study provided a new insight into the oxygen-sensing role of UQCRB in mitochondrial complex III.

### 2.4. Click chemistry

Affinity purification using biotin- or fluorescence-tagged small molecules is a powerful tool for target identification, but biotin- or fluorescence-modifications at the biologically active site of interest can result in a complete loss of activity. To overcome this problem, azide alkyne Huisgen cycloaddition chemistry (a common technique within so-called 'click chemistry') was adapted for target identification. The advantage of using this approach is that minimal structural modification is introduced to the small molecule of interest, without any loss of biological activity. Once the alkyne-derivatized small molecule is covalently bound to its target protein, a tag (e.g., fluorescein-azide or rhodamine-azide) can subsequently be attached via click chemistry.

Click chemistry was first adapted for live cell labeling by Bertozzi et al.[33] Jurkat cells were incubated with $Ac_4$-ManNAz to introduce SiaNAz residues into their cell-surface glycoproteins. Then, the azide-modified cell-surface glycoproteins were labeled with biotinylated cyclooctyne by using click chemistry. Therefore, the azide-modified cell-surface glycoproteins could be analyzed by flow cytometer with FITC-avidin. This is the first report to employ the reaction for the selective chemical modification of living cells.

Pezacki et al. used click chemistry reactions to identify the target protein of origamicin, an inhibitor of HCV replication.[34] Small molecules that interfere with host-viral interactions are potentially powerful tools for elucidating the molecular mechanisms of pathogenesis and defining new strategies for therapeutic development. Thus, Pezacki et al. screened for HCV replication inhibitors in their established ABA ((+)-S-abscisic acid) library based on the plant hormone ABA, a carotenoid-derived sesquiterpene. As a result, origamicin was identified as an HCV replication inhibitor. Because origamicin has an alkyne moiety in its structure, they exploited it to conjugate both rhodamine for in-gel fluorescence experiments and biotin for affinity chromatography experiments by using click chemistry. The purified protein from using biotinylated-origamicin was identified via LC–MS/MS as protein disulfide isomerase (PDI).

Stockwell et al. screened an inhibitor that suppresses cell death induced by polyglutamine-expanded huntingtin exon 1 (a cell-based model of Huntington's disease) from a 68,887 small-molecule library containing natural products and synthetic small molecules.[35] One hit was small molecule 16F16, and Stockwell et al. synthesized both biotin- and fluorescein-tagged 16F16. However, the modified 16F16 lost its biological activity, so they then used click chemistry. Lysates of PC12 were prepared and incubated with alkyne-derivatized 16F16 to bind to a target protein. Alkyne-derivatized 16F16 was coupled to rhodamine-azide via a click chemistry reaction. Next, fluorescent-tagged target proteins were affinity-purified, analyzed by SDS–PAGE and identified by MS as rat PDI (protein disulfide isomerase) precursors, PDIA1 and PDIA3. Expression of polyglutamine-expanded huntingtin exon 1 in PC12 cells caused PDI to concentrate at ER-mitochondrial junctions and triggered apoptosis via mitochondrial outer-membrane permeabilization. These studies demonstrated a novel strategy for identifying target proteins of small molecules.

### 2.5. Photo-crosslink

An additional method for overcoming the problem of a loss of biological activity of small molecules due to the presence of an affinity tag is photo-crosslink. Osada et al. developed this new method, which enables the introduction of a variety of small molecules onto solid supports through a photoaffinity reaction.[36] In this method, aryldiazirine groups covalently attached to solid supports are transformed upon UV irradiation into highly reactive carbenes, which are expected to bind to or insert irreversibly into proximal small molecules in a functional-group-independent manner. Osada et al. applied this method to methyl-gerfelin,[37] which had been found to suppress osteoclastogenesis. To understand the molecular mechanism by which this occurred, methyl-gerfelin was immobilized on agarose beads via a photoaffinity linker which they had developed. Binding proteins were purified and analyzed by MALDI-TOF MS, and glyoxalase I (GLO1) was identified as a methyl-gerfelin-binding protein. GLO1 knockdown interfered with osteoclast generation, and methyl-gerfelin competitively inhibited GLO1 enzymatic activity. These results suggest that methyl-gerfelin targets GLO1, resulting in the inhibition of osteoclastogenesis.

### 2.6. FG beads

Affinity purification using conventional matrices has several disadvantages, including nonspecific binding of irrelevant proteins to the affinity matrices and instability of these matrices. To overcome these issues, Handa and co-workers designed nonporous and physically stable, submicron-sized particles for affinity chromatography. In order to avoid nonspecific protein binding and to allow easy surface modification, they used polymer materials as components of the particles so that their surfaces possessed moderate hydrophilicity and an appropriate functional group. Based on these considerations, they developed high-performance affinity magnetic beads (FG beads)[38] and aimed to identify the target protein of thalidomide by using FG beads. Thalidomide was sold as a sedative in many countries and was often prescribed to pregnant women as a treatment for morning sickness. However, use of thalidomide causes multiple birth defects such as limb, ear, cardiac, and gastrointestinal malformations.[39–41] Despite considerable effort, little is known about the mechanisms underlying these developmental defects caused by thalidomide. Handa et al. identified cereblon (CRBN) as a thalidomide-binding protein by using FG beads.[42] CRBN was originally identified as a candidate gene for autosomal recessive mild mental retardation.[43] Although CRBN was reported to interact with DDB1,[44] which is a component of E3 ubiquitin ligase complexes containing Cullin 4 (Cul4A and Cul4B),[45] the functional relevance of this interaction remained unclear. Based on this information, they demonstrated that CRBN forms an E3 complex with DDB1 and Cul4A. Furthermore, thalidomide inhibited E3 ubiquitin ligase activity of the CRBN-containing complex due to its binding to CRBN. Next, to investigate whether the teratogenic effect of thalidomide could be observed in CRBN-knockdown animals, Handa et al. used zebrafish. CRBN-knockdown zebrafish by use of morpholino oligonucleotides exhibited specific defects in fin and otic vesicle development, which was a similar phenotype to those of thalidomide-treated embryos. Thus, thalidomide was shown to exert its teratogenic effects by binding to CRBN and inhibiting the associated ubiquitin ligase activity.

## 3. Indirect approach

Affinity chromatography is the most used and most successful method for identifying biological targets of multiple small molecules of interest. However, target identification using affinity chromatography begins with a structure–activity relationship (SAR) study, because we have to know which site(s) are nonessential to use as points of attachment to an affinity tag (e.g., biotin) or solid matrix (e.g., Affi-Gel agarose beads). Therefore, the primary limitation of affinity chromatography is the need to synthesize derivatives of small molecules. SAR studies are time-consuming and require extensive medicinal chemistry expertise. Furthermore, since biologically-active small molecules demonstrate vast structural diversity and complexity, many small molecules cannot be modified without affecting bioactivity, or cannot be easily obtained or synthesized in quantities large enough to permit SAR and subsequent studies. Because of these issues, target identification of small molecules using affinity chromatography is severely limited. This section highlights several 'Indirect Approaches' to overcome the limitations of the previously listed 'Direct Approaches' (Figs. 1B and 3).

### 3.1. DARTS (drug affinity responsive target stability)

To overcome the limitations of affinity chromatography described above, Huang and co-workers developed DARTS (Fig. 4). The strategy of DARTS is based on the principle that binding of drugs will stabilize target proteins, either globally or locally, for example, in a specific conformation or simply by masking protease recognition sites, thereby reducing the protease sensitivity of the target protein.[46–48] Thus, Huang et al. hypothesized that this could be exploited for target identification without requiring modification or immobilization of the small molecules. As a proof-of-principle, they first demonstrated that DARTS could identify FKBP12 as an FK506-binding protein.[49] Next, they aimed to apply DARTS to identify a molecular target of resveratrol, a small

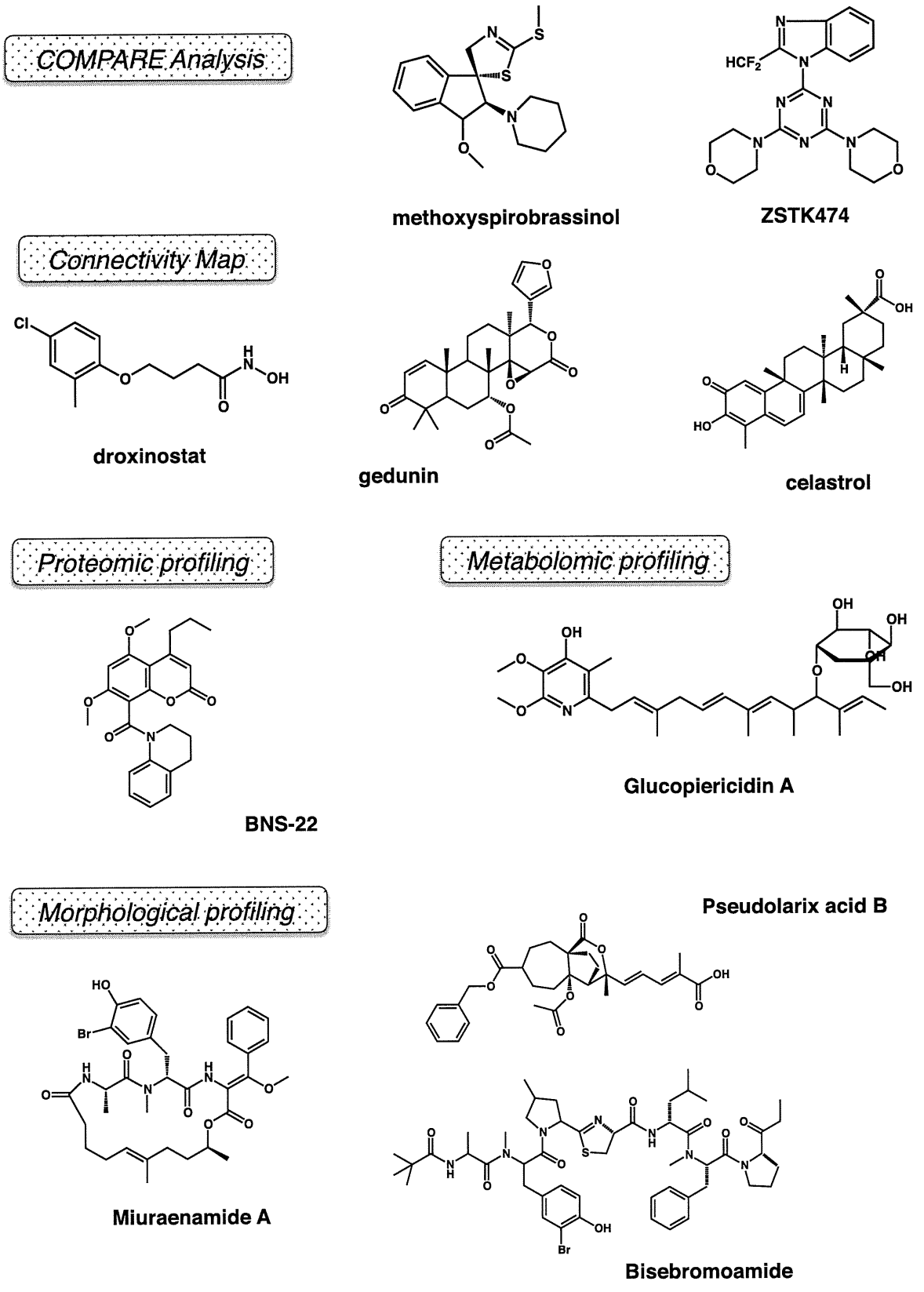


**Figure 3.** Structure of small molecules whose targets were identified by the 'Indirect Approach'.

molecule in red grapes and wine known for various health benefits including lifespan extension.[50]

Yeast cell lysates or human HeLa cell lysates were treated with resveratrol in vitro, followed by thermolysin digestion and silver staining after separation by SDS–PAGE. Bands of resveratrol-treated lysate protected from thermolysin digestion were analyzed by MS, and were identified as eIF4A (eukaryotic translation initiation factor 4A), a component required for the binding of mRNA to

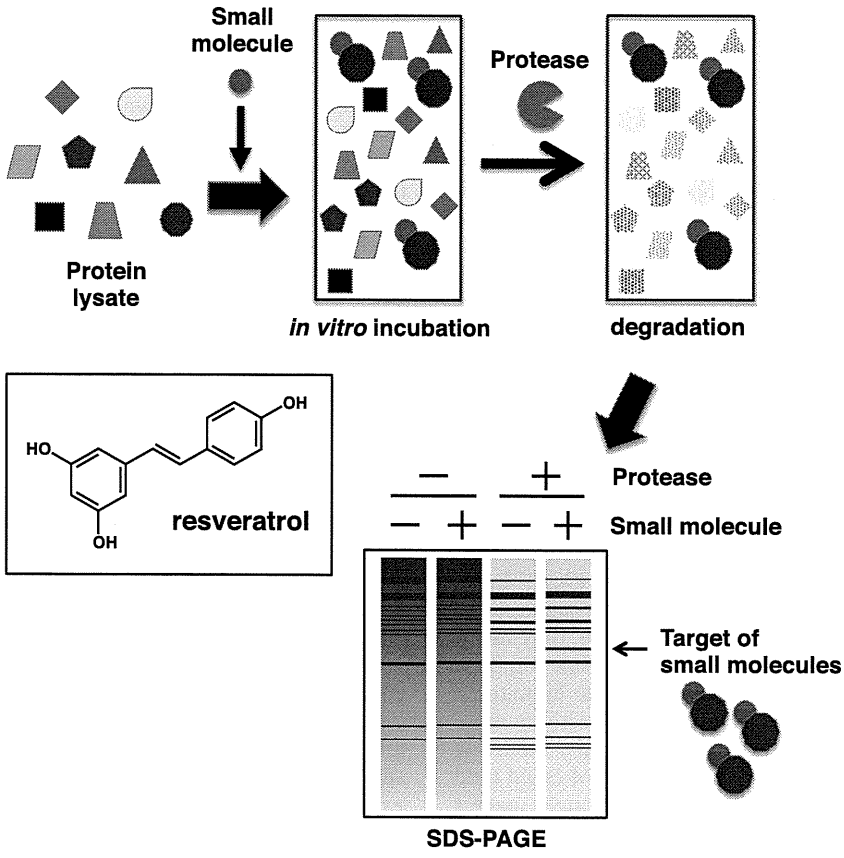


**Figure 4.** Schematic illustration of DARTS. Yeast or mammalian cultured cell lysates were prepared and treated with small molecules of interest in vitro, followed by protease digestion and silver staining after separation by SDS–PAGE.

40S ribosomal subunits. Purified wild-type eIF4A could be protected by resveratrol from proteolysis, suggesting that resveratrol directly bound to eIF4A. Furthermore, to address whether eIF4A is a target of resveratrol in vivo, they investigated the effect of resveratrol on EMCV IRES-mediated and HCV-mediated translation. Since it has been demonstrated that eIF4A is required for EMCV IRES-mediated translation but not HCV IRES-mediated translation, it follows that resveratrol inhibited EMCV-mediated but not HCV-mediated translation in HEK293 cells. These results indicated that resveratrol inhibited the biological function of eIF4A in vivo. On the other hand, because resveratrol extends lifespan,[50] they asked whether eIF4A is required for resveratrol's longevity effect. Whereas resveratrol lengthens the lifespan of wild-type N2 worms, this longevity effect is lost in eIF4A knockdown worms. These data suggested that eIF4A is a physiological target of resveratrol. Because DARTS does not require labeled small molecules and instead uses 'native' small molecules for binding, it is not limited by chemistry and can potentially be used for any small molecules.

### 3.2. Profiling

Apart from traditional target identification techniques such as affinity chromatography, new tools have emerged that can significantly aid mechanism elucidation efforts. The development of pattern matching algorithms that compare transcription profiles, drug susceptibility profiles, or morphological profile data, for example, to analogous data on compounds with known cellular targets, allow for mechanistic insights without the need to synthesize chemically-modified probes. Therefore, we next focus on new approaches using these pattern matching and chemical genomic tools.

### 3.3. COMPARE analysis

The National Cancer Institute established a panel of 60 human cancer cell lines (NCI60) derived from various organs. In a COMPARE analysis, the pattern of toxicity of small molecules to the NCI60 cell line panel is compared. Small molecules that have similar patterns of toxicity are highly correlated in the COMPARE algorithm; such a result suggests the small molecules have a similar mechanism of action, and indeed COMPARE has been successfully used in target identification studies. For example, 2-piperidyl analogues of natural indole phytoalexins, 1-methoxyspirobrassinols, and *N*-((1-benzyl-1*H*-1,2,3-trizol-4-yl)methyl)arylamide were reported to decrease intracellular glutathione levels[51] and inhibit tubulin polymerization,[52] respectively. Phytoalexins are small molecules naturally produced by plants. Various indole phytoalexins have been shown to exhibit anti-tumor activities. However, the anti-proliferative activity of most indole phytoalexins had been limited to certain cancer cells, and their mode of action has not been elucidated. Therefore, in order to achieve higher potency, new derivatives of indole phytoalexins have been synthesized. McDonald et al. synthesized 2-piperidyl analogues of indole phytoalexins, *cis*-1-Boc-, *trans*-1-Boc-, *cis*-1-methoxy- and *trans*-1-methoxy-2-deoxy-2-(1-piperidyl)spirobrassinols, and these derivatives exhibited a more favorable growth-inhibitory effect on some cancer cells than their parent compounds. Furthermore, to elucidate their mode of action, McDonald et al. performed COMPARE analysis with the NCI60 cell line panel. As a result, the profiles of their synthesized indole phytoalexins showed similar patterns with small molecules that deplete intracellular glutathione level, such as *N*-methylformamide and L-buthionine sulfoximine (BSO). Indeed, their synthesized indole phytoalexins decreased intracellular glutathione levels in

MCF-7 cells. Since glutathione is often involved in the resistance of cancer cells to radio- and chemotherapy, these small molecules with remarkable glutathione-depleting potency may be developed as radio- or chemo-sensitizing agents. A series of *N*-((1-benzyl-1*H*-1,2,3-trizol-4-yl)methyl)arylamides are synthetic derivatives of mycobactin S, a natural product produced by *Mycobacterium smegmatis* that exhibits anti-tuberculosis activity.[53] Moller et al. found that their synthesized derivatives showed anti-proliferative effects against human cancer cell lines. To evaluate the mode of action of *N*-((1-benzyl-1*H*-1,2,3-trizol-4-yl)methyl)arylamides, they performed COMPARE analysis with the NCI60 cell line panel. COMPARE analysis revealed that *N*-((1-benzyl-1*H*-1,2,3-trizol-4-yl)methyl)arylamides correlated with paclitaxel, vinblastine, and rhizoxin, all of which affect microtubule polymerization. Although further studies confirmed that *N*-((1-benzyl-1*H*-1,2,3-trizol-4-yl)methyl)arylamides inhibited microtubule polymerization in vitro and in vivo and induced G2/M cell cycle arrest, the mechanism by which *N*-((1-benzyl-1*H*-1,2,3-trizol-4-yl)methyl)arylamides inhibit microtubule polymerization still remains unclear.

Similar to the NCI60 cell line panel, Yamori et al. established a panel of 39 human cancer cell lines (termed JFCR39) coupled to a drug activity database. By using the JFCR39 database, they found that ZSTK474 exhibited similar responses to the PI3K inhibitor LY294002, suggesting that ZSTK474 is a new PI3K inhibitor.[54] Indeed, ZSTK474 was found to directly inhibit PI3K activity more efficiently than the PI3K inhibitor LY294002. Molecular modeling of the PI3K-ZSTK474 complex indicated that ZSTK474 could bind to the ATP-binding pocket of PI3K. These studies strongly suggest that this approach can be used to predict the molecular target or the mode of action of small molecules.

### 3.4. Connectivity Map database

Whole-genome transcript profiling has emerged as powerful tool to investigate the effects of small molecules on cells. The Connectivity Map database, developed at the Broad Institute, is a publicly accessible database comprised of gene expression data of cells treated with small molecules.[55] The transcript profile data of a compound of interest is compared to analogous data that has been collected on hundreds of small molecules with known molecular targets. The Connectivity Map database has been utilized in mode-of-action studies of several small molecules. For example, droxinostat was first identified as sensitizing malignant cells to the CH-11 Fas-activating antibody.[56] However, the Connectivity Map database revealed that the transcript profile of droxinostat showed a similar response to that of the HDAC inhibitors vorinostat and trichostatin A. Further cell-based and in vitro assays showed that droxinostat is a novel HDAC inhibitor that is selective for HDAC3, HDAC6, and HDAC8 through its hydroxamic acid moiety. To further explore the effects of HDAC inhibitions on Fas sensitization, Schimmer et al. knocked down HDACs with shRNA. As a result, HDAC8 knockdown enhanced sensitivity to Fas. Furthermore, droxinostat or HDAC8 knockdown was shown to decrease FLIP mRNA, a caspase-8 inhibitory protein. These results suggested that droxinostat decreased FLIP via HDAC inhibition, which resulted in sensitization to Fas-induced apoptosis. However, it is unclear whether HDACs inhibition by droxinostat would directly or indirectly decrease FLIP expression. Other examples include gedumin and celastrol. These two small molecules were identified as inhibitors of androgen receptor (AR)-activated signaling in prostate cancer by a high-throughput cell-based screening.[57] The Connectivity Map database revealed that these compounds were predicted to have a similar mode of action to the heat shock protein 90 (HSP90) inhibitors geldanamycin, 17-dimethylamino-geldanamycin and 17-allylaminogeldanamycin. It has been reported that the androgen receptor is a client of HSP90, and HSP90 inhibitors induced AR degradation. Thus, gedunin and celasteol were predicted to inhibit AR signaling by inhibiting HSP90. Indeed, these two compounds induced the down-regulation of AR and several other HSP90 client proteins. Furthermore, these two small molecules inhibited ATP binding to HSP90. However, since gedunin and celasteol did not compete for the ATP-binding site, gedunin and celasteol seem to have distinct mechanisms from geldanamycin. These studies suggested that the Connectivity Map database could also be used to predict the molecular target or the mode of action of small molecules.

### 3.5. Proteomic profiling

Compared with gene expression profiling like the Connectivity Map database which can simultaneously measure the expression of more than 20,000 genes, proteome analysis provides us with only ~1000 protein spots. However, two-dimensional gel electrophoresis (2DE) analyses often show us any change in molecular weight or isoelectric point of proteins after posttranslational modification as a clear mobility shift of protein spots. Because biologically active small molecules affect cellular processes and induce changes in both the expression level and modification of proteins, proteome profiling is an informative approach for investigating the effects of a small molecule. Osada and co-workers developed a new proteomic profiling system to predict the target protein of small molecules of interest.[58] To compare the proteomic pattern with small molecules whose targets are known, HeLa cells treated with each small molecule were analyzed by 2D-DIGE, and hierarchical clustering was performed. For example, radicicol and geldanamycin (structurally different HSP90 inhibitors), showed a similar proteome pattern, suggesting that this proteomic profiling system discriminates small molecules by mechanism of action. Indeed, the proteomic profiling analysis of BNS-22, a chemically synthesized derivative of the natural plant product GUT-70, showed that BNS-22 belongs to the same cluster as ICRF-193, a DNA topoisomerase II (TOP2) catalytic inhibitor. Further biochemical studies confirmed that BNS-22 targets and acts as a catalytic inhibitor of TOP2.[59]

### 3.6. Morphological profiling

A recent and rapidly developing technology is high content screening (HCS) that combines automated microscopy with image analysis, enabling phenotypic profiling of small molecules based on the activity of cells visualized by fluorescence cytology. Feng et al. introduced factor analysis as a data-driven tool for defining cell phenotypes and profiling small molecule activity.[60] They used a high-content image assay to screen and profile a library of 6547 small molecules derived from a diversity library (21%), a natural products library (58%) and a library of known bioactive small molecules (21%); all small molecules were assayed in HeLa cells to monitor cell proliferation, and to profile their cell cycle phenotype, using fluorescent probes for DNA (Hoechst 33342 dye), mitosis (anti-phosphoH3) and DNA replication (EdU; 5-ethyl-2-deoxyuridine). Images were automatically acquired and at least 500 cells were scored per treatment. They found that six factors (nuclear size, DNA replication, chromosome condensation, nuclear morphology, EdU texture, and nuclear shape) are sufficient to describe the biological responses. Profiling the small molecule library using these six factors resulted in the clustering of hits into seven phenotypic categories. Feng et al. then compared the phenotypic profiles, chemical similarity and predicted protein-binding activity of these small molecules. For instance, within the subcluster from the mitotic arrest phenotype, which is primarily characterized by high chromosome condensation, the authors observed four distinct

groups of structurally related small molecules; colchicine derivatives, a set of novel kinase inhibitors, quinolone derivatives and a pseudolarix acid B derivative. All of these small molecules have been reported to affect microtubules polymerization.[61–63] Indeed, they demonstrated depolymerization of microtubules and mitotic arrest in cells treated with each of the colchicine, quinolone and pseudolarix acid B derivatives.

Further cell morphological profiling has revealed bisebromoamide and miuraenamide A as actin filament stabilizers. Uesugi et al. used automated high-content image analysis to evaluate the morphology of cells exhibiting nuclear protrusion.[64] Actin-targeting small molecules decreased cytoplasmic area up to ~70%, and increased the distance between the centroid of the nucleus and the centroid of the entire cell. When those two parameters were plotted against each other, points for the seven known actin-targeting small molecules, cytochalasin D,[65] doliculide,[66] jasplakinolide,[67] latrunculin A,[68] mycalolide B,[69] seragamide A,[70] and swinholide A,[71] were clustered together. Based on this morphological profiling, the target of bisebromoamide and miuraenamide A, marine natural products whose targets were previously unknown,[72–75] were predicted to be actin stabilization. Indeed, they showed that bisebromoamide and miuraenamide A stabilized actin filaments in vitro, and fluorescein-conjugated bisebromoamide localized specifically to actin filaments in cells.

### 3.7. Metabolomics profiling

Metabolomic technologies have advanced tremendously in recent years, and capillary electrophoresis time-of-flight mass spectrometry (CE-TOFMS) has emerged as a powerful new tool for the comprehensive analysis of cellular metabolites.[76,77] The use of CE-TOFMS to understand global metabolism at the system level has become widespread.[78–81] Analysis of the metabolome with CE-TOFMS also reveals metabolic changes induced by small molecules. Thus, despite a lack of reports describing the identification of chemical inhibitor targets using metabolomic analysis, such efforts would be worthwhile. We screened bioactive compounds that inhibit cellular filopodia protrusion in carcinoma. Filopodia

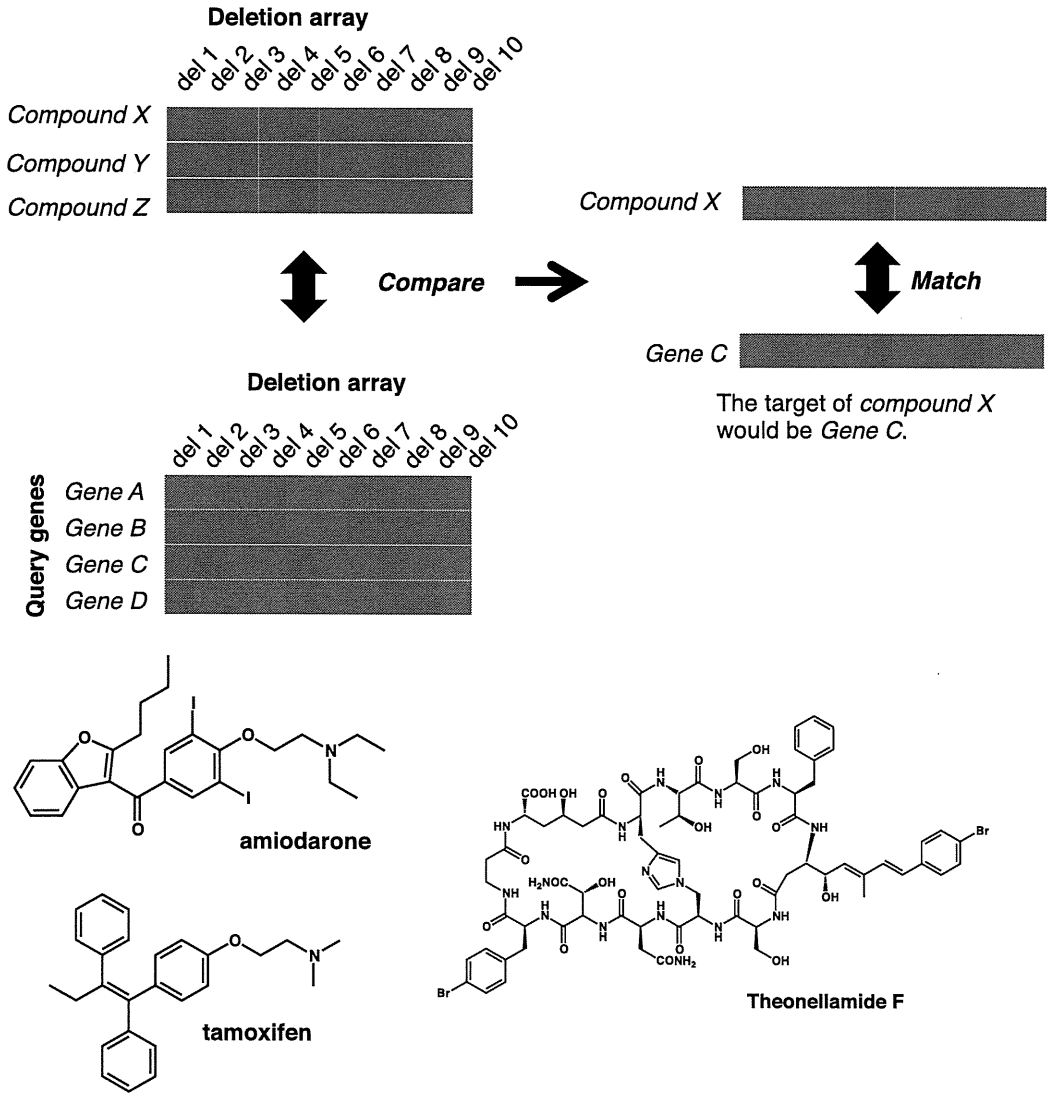


**Figure 5.** Comparison of a chemical-genetic profile to a compendium of genetic interaction (synthetic lethal) profiles could identify pathways and target genes of small molecules. Conceptually, the comparison of a chemical-genetic profile to the genetic interaction (synthetic lethal) profiles should identify the pathways and targets inhibited by small molecule treatment. For example, deletion mutants del2, del5, del6 and del8 are hypersensitive to compound X and a mutation in query *gene* C leads to a fitness defect when combined with deletion alleles del2, del5, del6 and del8. Here, the chemical-genetic profile of compound X resembles the genetic profile of *gene* C, thereby identifying the product of *gene* C as a putative target of compound X.

are spike-like cell membrane projections contributing to tumor metastasis; however, the molecular mechanisms controlling filopodia protrusion are complicated and unclear.[82,83] Thus, the discovery of a filopodia inhibitor and its molecular target which could be employed in chemical genetic studies may lead to a fuller understanding of filopodia, contributing to the treatment of tumor metastasis. In the course of screening filopodia protrusions from microbial origin, glucopiericidin A was isolated. Biochemical studies raised the possibility that glucopiericidin A would be an inhibitor of glycolysis. To address whether glucopiericidin A actually perturbs glycolysis, the effect of glucopiericidin A on global metabolism and on glycolysis was assessed by measuring the metabolome using CE-TOFMS. CE-TOFMS provided strong evidence that glucopiericidin A suppresses glycolysis by functionally targeting the glucose transporter. Our results represent a success of molecular target identification using metabolomics analysis.[84]

### 3.8. Chemical-genetic profiling in yeast

In yeast *Saccharomyces cerevisiae*, ~6000 potential genes have been characterized by the genome sequencing project. As each gene has been deleted, ~1000 essential genes and ~5000 viable deletion mutants were identified. Boone et al. generated a compendium of 'chemical-genetic interaction' profiles from scoring ~5000 viable yeast haploid deletion mutant strains for hypersensitivity to a diverse set of small molecules.[85] In addition, they also generated 'genetic interaction (synthetic lethal)' profiles by testing viabilities in each double gene-mutant combination. Conceptually, the comparison of a chemical-genetic profile to the genetic interaction (synthetic lethal) profile should identify the pathways and targets inhibited by small molecule treatment (Fig. 5).

Boone et al. generated chemical-genetic profiles for 82 different conditions by testing the collection of viable yeast haploid deletion mutants for hypersensitivity to 82 small molecules, including 75 synthetic and natural products and 7 crude antifungal extracts derived from different marine sponges and microorganisms.[86] The set of chemical-genetic profiles, visualized by two-dimensional hierarchical clustering, revealed that small molecules with similar cellular effects showed similar chemical-genetic profiles. Examples include (i) actin binding agents latrunculin B[87] and cytochalasin A;[88] (ii) cell wall synthesis inhibitors staurosporine, which targets protein kinase C, a regulator of a MAP kinase cascade involved in cell wall metabolism,[89] and caspofungin, which inhibits 1,3 β-glucan synthase;[90] (iii) radicicol and geldanamycin—although structurally unrelated, both act as highly selective inhibitors of Hsp90 function through their ability to bind within the ADP/ATP binding pocket of the chaperone.[91] Interestingly, the chemical-genetic interactions of amiodarone, an antifungal and anti-arrhythmic small molecule, clusters with tamoxifen, a competitive inhibitor of estradiol binding to the estrogen receptor and a common breast cancer drug. This is notable, as the antifungal activity of amiodarone is the perturbation of calcium homeostasis,[92] and tamoxifen seems to produce an increase in cytosolic $Ca^{2+}$ in yeast. Indeed, both amiodarone and tamoxifen triggered the reporter activity driven by calcineurin-dependent response element (CDRE), suggesting that tamoxifen is a potent activator of calcineurin signaling. Furthermore, two natural product extracts (prior to purification of the active component) that were derived from different organisms and diverse locations, from a sea cucumber from the Commonwealth of Dominica and an Indonesian marine sponge, showed highly similar chemical-genetic profiles. After purification, the active components were identical to stichloroside[93] and theopalauamide,[94] respectively. Both of the purified small molecules display chemical-genetic profiles resembling those of their crude extracts, suggesting that chemical-genetic profiling is an effective means for functional classification of natural product extracts. Taken together, Boone et al. demonstrated the potential for integration of chemical-genetic profiles and genetic interaction profiles to provide information about the pathways and targets affected by bioactive small molecules.

Another example was reported by Yoshida et al.[95] Theonellamides are members of a unique family of bicyclic dodecapeptides isolated from a marine sponge, *Theonella* sp. These small molecules show broad antifungal activity as well as moderate cytotoxicity in mammalian cells.[96,97] Despite screens for binding proteins using theonellamide A affinity beads, their target molecules remain unknown.[98] Therefore, to evaluate the mode of action of theonellamide, Yoshida et al. generated a chemical-genomic profile of theonellamide F, bicyclic peptides derived from a marine sponge, using a collection of fission yeast strains in which each open reading frame (ORF) is expressed under the control of an inducible promoter (fission yeast ORFeome overexpression strain collection).[99,100] The overexpression strains were exposed individually to theonellamide F and a compendium of 10 reference small molecules with known targets at various concentrations. Strains showing a significantly altered sensitivity compared to the control strain were selected. Cluster analysis of the Gene Ontology (GO) terms associated with the genes that alter small molecule sensitivity suggested a mechanistic link between theonellamide and 1,3-β-D-glucan synthesis. Overproduction of 1,3-β-D-glucan was induced by theonellamide F in a Rho1-dependent manner. Furthermore, by using a fluorescent theonellamide derivative, theonellamides were shown to specifically bind in vitro to 3β-hydroxysterols, including ergosterol, and cause membrane damage. Taken together, these results show that theonellamides are a new class of sterol-binding molecules that induce membrane damage and activate Rho1-mediated 1,3-β-D-glucan synthesis.

## Acknowledgements

We are grateful to Ms. Yukiko Sasazawa, Ms. Satoko Shinjo, Mr. Kohta Yamamoto, Mr. Shigeyuki Magi, and Mr. Takahiro Fujimaki for supporting some of our work.

## References and notes

1. Pandey, A.; Mann, M. *Nature* **2000**, *405*, 837.
2. Alaimo, P. J.; Shogren-Knaak, M. A.; Shokat, K. M. *Curr. Opin. Chem. Biol.* **2001**, *5*, 360.
3. Zheng, X. F.; Chan, T. F. *Drug Discovery Today* **2002**, *7*, 197.
4. Kino, T.; Hatanaka, H.; Hashimoto, M.; Nishiyama, M.; Goto, T.; Okuhara, M.; Kohsaka, M.; Aoki, H.; Imanaka, H. *J. Antibiot. (Tokyo)* **1987**, *40*, 1249.
5. Siekierka, J. J.; Hung, S. H.; Poe, M.; Lin, C. S.; Sigal, N. H. *Nature* **1989**, *341*, 755.
6. Liu, J.; Farmer, J. D., Jr.; Lane, W. S.; Friedman, J.; Weissman, I.; Schreiber, S. L. *Cell* **1991**, *66*, 807.
7. Omura, S.; Fujimoto, T.; Otoguro, K.; Matsuzaki, K.; Moriguchi, R.; Tanaka, H.; Sasaki, Y. *J. Antibiot. (Tokyo)* **1991**, *44*, 113.
8. Fenteany, G.; Standaert, R. F.; Lane, W. S.; Choi, S.; Corey, E. J.; Schreiber, S. L. *Science* **1995**, *268*, 726.
9. Jensen, T. J.; Loo, M. A.; Pind, S.; Williams, D. B.; Goldberg, A. L.; Riordan, J. R. *Cell* **1995**, *83*, 129.
10. Lee, D. H.; Goldberg, A. L. *Trends Cell Biol.* **1998**, *8*, 397.
11. Hart, C. P. *Drug Discovery Today* **2005**, *10*, 513.
12. Galat, A.; Lane, W. S.; Standaert, R. F.; Schreiber, S. L. *Biochemistry* **1992**, *31*, 2427.
13. Choi, Y.; Shimogawa, H.; Murakami, K.; Ramdas, L.; Zhang, W.; Qin, J.; Uesugi, M. *Chem. Biol.* **2006**, *13*, 241.
14. Falsey, R. R.; Marron, M. T.; Gunaherath, G. M.; Shirahatti, N.; Mahadevan, D.; Gunatilaka, A. A.; Whitesell, L. *Nat. Chem. Biol.* **2006**, *2*, 33.
15. Kahsai, A. W.; Cui, J.; Kaniskan, H. U.; Garner, P. P.; Fenteany, G. *J. Biol. Chem.* **2008**, *283*, 24534.
16. Kaida, D.; Motoyoshi, H.; Tashiro, E.; Nojima, T.; Hagiwara, M.; Ishigami, K.; Watanabe, H.; Kitahara, T.; Yoshida, T.; Nakajima, H., et al *Nat. Chem. Biol.* **2007**, *3*, 576.
17. Kotake, Y.; Sagane, K.; Owa, T.; Mimori-Kiyosue, Y.; Shimizu, H.; Uesugi, M.; Ishihama, Y.; Iwata, M.; Mizui, Y. *Nat. Chem. Biol.* **2007**, *3*, 570.
18. Kamisuki, S.; Mao, Q.; Abu-Elheiga, L.; Gu, Z.; Kugimiya, A.; Kwon, Y.; Shinohara, T.; Kawazoe, Y.; Sato, S.; Asakura, K., et al *Chem. Biol.* **2009**, *16*, 882.

19. Choi, Y.; Kawazoe, Y.; Murakami, K.; Misawa, H.; Uesugi, M. *J. Biol. Chem.* **2003**, *278*, 7320.
20. Kahsai, A. W.; Zhu, S.; Wardrop, D. J.; Lane, W. S.; Fenteany, G. *Chem. Biol.* **2006**, *13*, 973.
21. Tsukita, S.; Hieda, Y. *J. Cell Biol.* **1989**, *108*, 2369.
22. Nakajima, H.; Sato, B.; Fujita, T.; Takase, S.; Terano, H.; Okuhara, M. *J. Antibiot. (Tokyo)* **1996**, *49*, 1196.
23. Nakajima, H.; Hori, Y.; Terano, H.; Okuhara, M.; Manda, T.; Matsumoto, S.; Shimomura, K. *J. Antibiot. (Tokyo)* **1996**, *49*, 1204.
24. Mizui, Y.; Sakai, T.; Iwata, M.; Uenaka, T.; Okamoto, K.; Shimizu, H.; Yamori, T.; Yoshimatsu, K.; Asada, M. *J. Antibiot. (Tokyo)* **2004**, *57*, 188.
25. Sakai, T.; Sameshima, T.; Matsufuji, M.; Kawamura, N.; Dobashi, K.; Mizui, Y. *J. Antibiot. (Tokyo)* **2004**, *57*, 173.
26. Sakai, T.; Asai, N.; Okuda, A.; Kawamura, N.; Mizui, Y. *J. Antibiot. (Tokyo)* **2004**, *57*, 180.
27. Chen, S.; Do, J. T.; Zhang, Q.; Yao, S.; Yan, F.; Peters, E. C.; Scholer, H. R.; Schultz, P. G.; Ding, S. *Proc. Natl. Acad. Sci. U.S.A.* **2006**, *103*, 17266.
28. Yang, J.; Shamji, A.; Matchacheep, S.; Schreiber, S. L. *Chem. Biol.* **2007**, *14*, 371.
29. Palacios, F.; Schweitzer, J. K.; Boshans, R. L.; D'Souza-Schorey, C. *Nat. Cell Biol.* **2002**, *4*, 929.
30. Jung, H. J.; Lee, H. B.; Kim, C. J.; Rho, J. R.; Shin, J.; Kwon, H. J. *J. Antibiot. (Tokyo)* **2003**, *56*, 492.
31. Jung, H. J.; Shim, J. S.; Lee, J.; Song, Y. M.; Park, K. C.; Choi, S. H.; Kim, N. D.; Yoon, J. H.; Mungai, P. T.; Schumacker, P. T., et al *J. Biol. Chem.* **2010**, *285*, 11584.
32. Suzuki, H.; Hosokawa, Y.; Toda, H.; Nishikimi, M.; Ozawa, T. *Biochem. Biophys. Res. Commun.* **1988**, *156*, 987.
33. Agard, N. J.; Prescher, J. A.; Bertozzi, C. R. *J. Am. Chem. Soc.* **2004**, *126*, 15046.
34. Rakic, B.; Clarke, J.; Tremblay, T. L.; Taylor, J.; Schreiber, K.; Nelson, K. M.; Abrams, S. R.; Pezacki, J. P. *Chem. Biol.* **2006**, *13*, 1051.
35. Hoffstrom, B. G.; Kaplan, A.; Letso, R.; Schmid, R. S.; Turmel, G. J.; Lo, D. C.; Stockwell, B. R. *Nat. Chem. Biol.* **2010**, *6*, 900.
36. Kanoh, N.; Kumashiro, S.; Simizu, S.; Kondoh, Y.; Hatakeyama, S.; Tashiro, H.; Osada, H. *Angew. Chem., Int. Ed.* **2003**, *42*, 5584.
37. Kawatani, M.; Okumura, H.; Honda, K.; Kanoh, N.; Muroi, M.; Dohmae, N.; Takami, M.; Kitagawa, M.; Futamura, Y.; Imoto, M., et al *Proc. Natl. Acad. Sci. U.S.A.* **2008**, *105*, 11691.
38. Sakamoto, S.; Kabe, Y.; Hatakeyama, M.; Yamaguchi, Y.; Handa, H. *Chem. Rec.* **2009**, *9*, 66.
39. Miller, M. T.; Stromland, K. *Teratology* **1999**, *60*, 306.
40. Melchert, M.; List, A. *Int. J. Biochem. Cell Biol.* **2007**, *39*, 1489.
41. Knobloch, J.; Ruther, U. *Cell Cycle* **2008**, *7*, 1121.
42. Ito, T.; Ando, H.; Suzuki, T.; Ogura, T.; Hotta, K.; Imamura, Y.; Yamaguchi, Y.; Handa, H. *Science* **2010**, *327*, 1345.
43. Higgins, J. J.; Pucilowska, J.; Lombardi, R. Q.; Rooney, J. P. *Neurology* **2004**, *63*, 1927.
44. Angers, S.; Li, T.; Yi, X.; MacCoss, M. J.; Moon, R. T.; Zheng, N. *Nature* **2006**, *443*, 590.
45. Groisman, R.; Polanowska, J.; Kuraoka, I.; Sawada, J.; Saijo, M.; Drapkin, R.; Kisselev, A. F.; Tanaka, K.; Nakatani, Y. *Cell* **2003**, *113*, 357.
46. Park, C.; Marqusee, S. *Nat. Methods* **2005**, *2*, 207.
47. Stankunas, K.; Bayle, J. H.; Gestwicki, J. E.; Lin, Y. M.; Wandless, T. J.; Crabtree, G. R. *Mol. Cell* **2003**, *12*, 1615.
48. Tucker, C. L.; Fields, S. *Nat. Biotechnol.* **2001**, *19*, 1042.
49. Lomenick, B.; Hao, R.; Jonai, N.; Chin, R. M.; Aghajan, M.; Warburton, S.; Wang, J.; Wu, R. P.; Gomez, F.; Loo, J. A., et al *Proc. Natl. Acad. Sci. U.S.A.* **2009**, *106*, 21984.
50. Wood, J. G.; Rogina, B.; Lavu, S.; Howitz, K.; Helfand, S. L.; Tatar, M.; Sinclair, D. *Nature* **2004**, *430*, 686.
51. Mezencev, R.; Kutschy, P.; Salayova, A.; Curillova, Z.; Mojzis, J.; Pilatova, M.; McDonald, J. *Chemotherapy* **2008**, *54*, 372.
52. Stefely, J. A.; Palchaudhuri, R.; Miller, P. A.; Peterson, R. J.; Moraski, G. C.; Hergenrother, P. J.; Miller, M. J. *J. Med. Chem.* **2010**, *53*, 3389.
53. Maurer, P. J.; Miller, M. J. *J. Am. Chem. Soc.* **1983**, *105*, 240.
54. Yaguchi, S.; Fukui, Y.; Koshimizu, I.; Yoshimi, H.; Matsuno, T.; Gouda, H.; Hirono, S.; Yamazaki, K.; Yamori, T. *J. Natl. Cancer Inst.* **2006**, *98*, 545.
55. Lamb, J.; Crawford, E. D.; Peck, D.; Modell, J. W.; Blat, I. C.; Wrobel, M. J.; Lerner, J.; Brunet, J. P.; Subramanian, A.; Ross, K. N., et al *Science* **2006**, *313*, 1929.
56. Wood, T. E.; Dalili, S.; Simpson, C. D.; Sukhai, M. A.; Hurren, R.; Anyiwe, K.; Mao, X.; Suarez Saiz, F.; Gronda, M.; Eberhard, Y., et al *Mol. Cancer Ther.* **2010**, *9*, 246.
57. Hieronymus, H.; Lamb, J.; Ross, K. N.; Peng, X. P.; Clement, C.; Rodina, A.; Nieto, M.; Du, J.; Stegmaier, K.; Raj, S. M., et al *Cancer Cell* **2006**, *10*, 321.
58. Muroi, M.; Kazami, S.; Noda, K.; Kondo, H.; Takayama, H.; Kawatani, M.; Usui, T.; Osada, H. *Chem. Biol.* **2010**, *17*, 460.
59. Kawatani, M.; Takayama, H.; Muroi, M.; Kimura, S.; Maekawa, T.; Osada, H. *Chem. Biol.* **2011**, *18*, 743.
60. Young, D. W.; Bender, A.; Hoyt, J.; McWhinnie, E.; Chirn, G. W.; Tao, C. Y.; Tallarico, J. A.; Labow, M.; Jenkins, J. L.; Mitchison, T. J., et al *Nat. Chem. Biol.* **2008**, *4*, 59.
61. Li, L.; Wang, H. K.; Kuo, S. C.; Wu, T. S.; Mauger, A.; Lin, C. M.; Hamel, E.; Lee, K. H. *J. Med. Chem.* **1994**, *37*, 3400.
62. Shi, Q.; Chen, K.; Morris-Natschke, S. L.; Lee, K. H. *Curr. Pharm. Des.* **1998**, *4*, 219.
63. Tong, Y. G.; Zhang, X. W.; Geng, M. Y.; Yue, J. M.; Xin, X. L.; Tian, F.; Shen, X.; Tong, L. J.; Li, M. H.; Zhang, C., et al *Mol. Pharmacol.* **2006**, *69*, 1226.
64. Sumiya, E.; Shimogawa, H.; Sasaki, H.; Tsutsumi, M.; Yoshita, K.; Ojika, M.; Suenaga, K.; Uesugi, M. *ACS Chem. Biol.* **2011**, *6*, 425.
65. Flanagan, M. D.; Lin, S. *J. Biol. Chem.* **1980**, *255*, 835.
66. Bai, R.; Covell, D. G.; Liu, C.; Ghosh, A. K.; Hamel, E. *J. Biol. Chem.* **2002**, *277*, 32165.
67. Bubb, M. R.; Senderowicz, A. M.; Sausville, E. A.; Duncan, K. L.; Korn, E. D. *J. Biol. Chem.* **1994**, *269*, 14869.
68. Coue, M.; Brenner, S. L.; Spector, I.; Korn, E. D. *FEBS Lett.* **1987**, *213*, 316.
69. Saito, S.; Watabe, S.; Ozaki, H.; Fusetani, N.; Karaki, H. *J. Biol. Chem.* **1994**, *269*, 29710.
70. Tanaka, C.; Tanaka, J.; Bolland, R. F.; Marriott, G.; Higa, T. *Tetrahedron* **2006**, 62.
71. Bubb, M. R.; Spector, I.; Bershadsky, A. D.; Korn, E. D. *J. Biol. Chem.* **1995**, *270*, 3463.
72. Ojika, M.; Inukai, Y.; Kito, Y.; Hirata, M.; Iizuka, T.; Fudou, R. *Chem. Asian J.* **2008**, *3*, 126.
73. Iizuka, T.; Fudou, R.; Jojima, Y.; Ogawa, S.; Yamanaka, S.; Inukai, Y.; Ojika, M. *J. Antibiot. (Tokyo)* **2006**, *59*, 385.
74. Teruya, T.; Sasaki, H.; Fukazawa, H.; Suenaga, K. *Org. Lett.* **2009**, *11*, 5062.
75. Gao, X.; Liu, Y.; Kwong, S.; Xu, Z.; Ye, T. *Org. Lett.* **2010**, *12*, 3018.
76. Soga, T.; Ohashi, Y.; Ueno, Y.; Naraoka, H.; Tomita, M.; Nishioka, T. *J. Proteome Res.* **2003**, *2*, 488.
77. Monton, M. R.; Soga, T. *J. Chromatogr., A* **2007**, *1168*, 237. discussion 236.
78. Hirayama, A.; Kami, K.; Sugimoto, M.; Sugawara, M.; Toki, N.; Onozuka, H.; Kinoshita, T.; Saito, N.; Ochiai, A.; Tomita, M., et al *Cancer Res.* **2009**, *69*, 4918.
79. Ishii, N.; Nakahigashi, K.; Baba, T.; Robert, M.; Soga, T.; Kanai, A.; Hirasawa, T.; Naba, M.; Hirai, K.; Hoque, A., et al *Science* **2007**, *316*, 593.
80. Soga, T.; Baran, R.; Suematsu, M.; Ueno, Y.; Ikeda, S.; Sakurakawa, T.; Kakazu, Y.; Ishikawa, T.; Robert, M.; Nishioka, T., et al *J. Biol. Chem.* **2006**, *281*, 16768.
81. Sugimoto, M.; Wong, D. T.; Hirayama, A.; Soga, T.; Tomita, M. *Metabolomics* **2010**, *6*, 78.
82. Faix, J.; Rottner, K. *Curr. Opin. Cell Biol.* **2006**, *18*, 18.
83. Mattila, P. K.; Lappalainen, P. *Nat. Rev. Mol. Cell Biol.* **2008**, *9*, 446.
84. Kitagawa, M.; Ikeda, S.; Tashiro, E.; Soga, T.; Imoto, M. *Chem. Biol.* **2010**, *17*, 989.
85. Parsons, A. B.; Brost, R. L.; Ding, H.; Li, Z.; Zhang, C.; Sheikh, B.; Brown, G. W.; Kane, P. M.; Hughes, T. R.; Boone, C. *Nat. Biotechnol.* **2004**, *22*, 62.
86. Parsons, A. B.; Lopez, A.; Givoni, I. E.; Williams, D. E.; Gray, C. A.; Porter, J.; Chua, G.; Sopko, R.; Brost, R. L.; Ho, C. H., et al *Cell* **2006**, *126*, 611.
87. Ayscough, K. R.; Stryker, J.; Pokala, N.; Sanders, M.; Crews, P.; Drubin, D. G. *J. Cell Biol.* **1997**, *137*, 399.
88. Torralba, S.; Raudaskoski, M.; Pedregosa, A. M.; Laborda, F. *Microbiology* **1998**, *144*, 45.
89. Yoshida, S.; Ikeda, E.; Uno, I.; Mitsuzawa, H. *Mol. Gen. Genet.* **1992**, *231*, 337.
90. Douglas, C. M.; Marrinan, J. A.; Li, W.; Kurtz, M. B. *J. Bacteriol.* **1994**, *176*, 5686.
91. Roe, S. M.; Prodromou, C.; O'Brien, R.; Ladbury, J. E.; Piper, P. W.; Pearl, L. H. *J. Med. Chem.* **1999**, *42*, 260.
92. Gupta, S. S.; Ton, V. K.; Beaudry, V.; Rulli, S.; Cunningham, K.; Rao, R. *J. Biol. Chem.* **2003**, *278*, 28831.
93. Kitagawa, I.; Kobayashi, M.; Imamoto, T.; Yasuzawa, T.; Kyogoku, Y. *Chem. Pharm. Bull.* **1981**, *29*, 2387.
94. Schmidt, E. W.; Bewley, C. A.; Faulkner, D. J. *J. Org. Chem.* **1998**, *63*, 1254.
95. Nishimura, S.; Arita, Y.; Honda, M.; Iwamoto, K.; Matsuyama, A.; Shirai, A.; Kawasaki, H.; Kakeya, H.; Kobayashi, T.; Matsunaga, S., et al *Nat. Chem. Biol.* **2010**, *6*, 519.
96. Matsunaga, S.; Fusetani, N. *J. Org. Chem.* **1995**, *60*, 1177.
97. Matsunaga, S.; Fusetani, N.; Hashimoto, K.; Walchli, M. *J. Am. Chem. Soc.* **1989**, *111*, 2582.
98. Wada, S.; Matsunaga, S.; Fusetani, N.; Watabe, S. *Mar. Biotechnol. (NY)* **2000**, *2*, 285.
99. Matsuyama, A.; Arai, R.; Yashiroda, Y.; Shirai, A.; Kamata, A.; Sekido, S.; Kobayashi, Y.; Hashimoto, A.; Hamamoto, M.; Hiraoka, Y., et al *Nat. Biotechnol.* **2006**, *24*, 841.
100. Shirai, A.; Matsuyama, A.; Yashiroda, Y.; Hashimoto, A.; Kawamura, Y.; Arai, R.; Komatsu, Y.; Horinouchi, S.; Yoshida, M. *J. Biol. Chem.* **2008**, *283*, 10745.

The Journal of Antibiotics (2012) 65, 211–214

www.nature.com/ja

NOTE

# Napyradiomycin A1, an inhibitor of mitochondrial complexes I and II

Kohta Yamamoto[1], Etsu Tashiro[1], Keiichiro Motohashi[2], Haruo Seto[2] and Masaya Imoto[1]

*The Journal of Antibiotics* (2012) **65**, 211–214; doi:10.1038/ja.2011.138; published online 18 January 2012

**Keywords:** mitochondrial electron transport; napyradiomycin; intracellular ATP level

We have previously proposed a cell-based screening method 'EGF-induced (epidermal growth factor) filopodium protrusion assay' to identify mitochondrial electron transport inhibitors or glycolysis inhibitors. Filopodia are spike-like cell membrane projections that contribute to tumor metastasis. Previously, we have reported that mitochondrial electron transport inhibition resulted in the inhibition of EGF-induced filopodium protrusion in human adenocarcinoma A431 cells only when their glycolytic pathways were restricted.[1] By using the inhibition of filopodium protrusion as an indicator, we identified napyradiomycin A1 (Figure 1a; isolated from *Streptomyces antimycoticus* NT17),[2] which was previously identified as an antibacterial antibiotic,[3] as a candidate of mitochondrial electron transport inhibitor. A431 cells were treated with napyradiomycin A1 with or without 10 mM 2-deoxy-D-glucose (Sigma-Aldrich, St Louis, MO, USA) for 30 min, followed by 30 ng ml$^{-1}$ EGF (Sigma-Aldrich) stimulation and observation under a microscope. As shown in Figure 1b, 20 μM napyradiomycin A1 inhibited EGF-induced filopodium protrusion in A431 cells only in the presence of the glycolytic enzyme hexokinase inhibitor 2-deoxy-D-glucose. Mitochondrial electron transport inhibitor rotenone (Sigma-Aldrich) also inhibited filopodium protrusion only in the presence of 2-deoxy-D-glucose. Furthermore, it was reported that co-treatment with a mitochondrial electron transport inhibitor and a glycolytic inhibitor markedly decreased intracellular ATP levels.[1] We then tested whether napyradiomycin A1 decreased ATP levels in A431 cells in which glycolytic pathways were restricted. As intracellular ATP levels were not affected by EGF stimulation (data not shown), we measured intracellular ATP levels under the condition where A431 cells were treated with napyradiomycin A1 with or without 10 mM 2-deoxy-D-glucose for 30 min in the absence of EGF. After incubation, intracellular ATP levels were measured using a Cell Titer-Glo Luminescent Cell Viability Assay Kit (Promega, Madison, WI, USA) with a luminometer (Wallac; Perkin-Elmer, Waltham, MA, USA). As shown in Figure 1c, napyradiomycin A1 treatment did not decrease cellular ATP levels; however, 20 μM napyradiomycin A1 markedly decreased cellular ATP levels in the presence of 2-deoxy-D-glucose in A431 cells. Furthermore, ATP levels in HeLa cells also decreased under co-treatment with napyradiomycin A1 and 2-deoxy-D-glucose (data not shown). These results suggested that napyradiomycin A1 inhibited mitochondrial electron transport in cancer cells.

Next, we examined whether napyradiomycin A1 actually inhibited mitochondrial electron transport *in vitro* by using submitochondrial particles (SMP) obtained from the bovine heart. In order to prepare SMP, bovine hearts were homogenized in MSH buffer (210 mM mannitol, 70 mM sucrose, 1 mM DTT, 1 mM EGTA, 0.1% BSA and 10 mM HEPES pH 7.4) with a Potter-Elvehjem homogenizer (Nippon genetics, Tokyo, Japan). Homogenates were centrifuged at 1000 *g* for 10 min, and the resulting supernatant was further centrifuged at 8000 *g* for 20 min. Pellets were suspended in MSH buffer and obtained as SMP.[4]

The mitochondrial electron transport chain consists of four discrete multisubunit complexes: NADH–ubiquinone oxidoreductase (complex I), succinate–ubiquinone oxidoreductase (complex II), ubiquinol–cytochrome *c* oxidoreductase (complex III) and cytochrome *c* oxidase (complex IV). Therefore, we evaluated which complex was the target of napyradiomycin A1.

Mitochondrial complex I activity was measured by monitoring the absorbance change of NADH at 340 nm in the presence of antimycin A (Sigma-Aldrich) and KCN (Sigma-Aldrich), an inhibitor of complex III and complex IV, respectively.[5,6] The enzyme assay was performed at 30 °C in a buffer containing 50 mM phosphate (pH 7.4), 250 mM sucrose, 0.1 μg ml$^{-1}$ antimycin A, 2 mM KCN, 50 μM decylubiquinone (DB; 2,3-dimethoxy-5-methyl-6-decyl-1,4-benzoquinone, an exogenous hydrophobic quinone that acts as electron acceptor; Sigma-Aldrich),[7] 0.2 mM NADH, and 12 μg ml$^{-1}$ SMP with or without napyradiomycin A1. Rotenone was used as a positive control of complex I inhibitor. We found that napyradiomycin A1 inhibited complex I activity with an $IC_{50}$ value of 20 μM (Figure 2a).

[1]Chemical Biology Laboratory, Department of Biosciences and Informatics, Faculty of Science and Technology, Keio University, Yokohama City, Japan and [2]Bioregulatory Laboratory, Faculty of Applied Biosciences, Tokyo University of Agriculture, Tokyo, Japan
Correspondence: Dr E Tashiro, Department of Biosciences and Informatics, Faculty of Science and Technology, Chemical Biology Laboratory, Faculty of Science and Technology, Keio University, 3-14-1 Hiyoshi, Kohoku-ku, Yokohama 223-8522, Japan.
E-mail: tashiro@bio.keio.ac.jp
Received 2 December 2011; revised 15 December 2011; accepted 16 December 2011; published online 18 January 2012

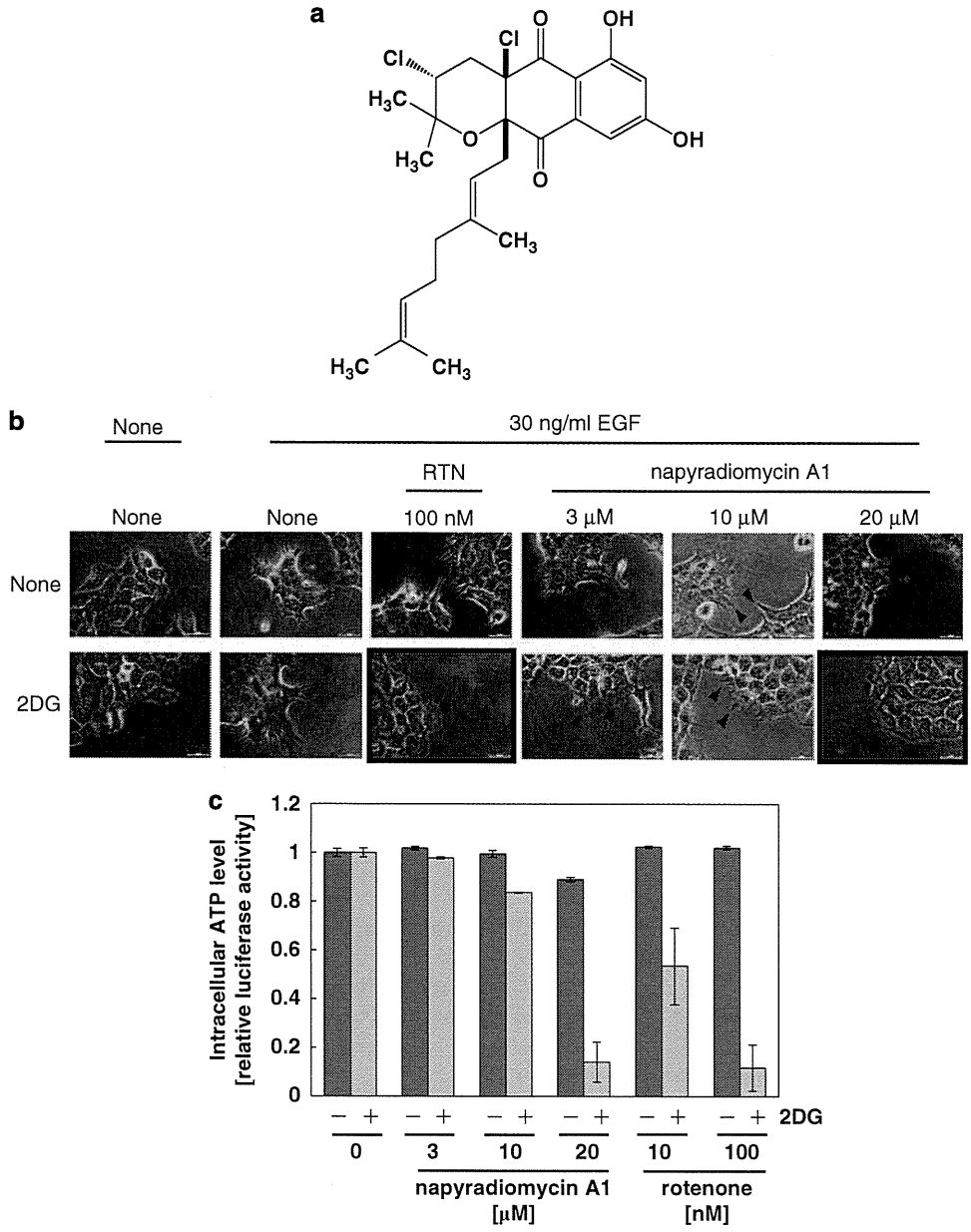


**Figure 1** Napyradiomycin A1 decreased intracellular ATP levels. (**a**) The structure of napyradiomycin A1.[3] (**b**) Napyradiomycin A1 inhibited EGF-induced filopodia protrusion only in the presence of 2-deoxy-D-glucose (2DG, 10 mM). The assay method was as described previously.[1] Mitochondrial electron transport inhibitor rotenone (RTN 100 nM) was used as a positive control. Arrowhead indicates filopodia, and the framed photos show filopodium inhibition. (**c**) Napyradiomycin A1 decreased intracellular ATP levels in 2DG-treated A431 cells. A431 cells were treated with napyradiomycin A1 with or without 10 mM of 2DG for 30 min. After incubation, intracellular ATP levels were measured using a Cell Titer-Glo Luminescent Cell Viability Assay Kit with a luminometer.

Mitochondrial complex II activity was measured by monitoring the absorbance change of 2,6-dichlorophenolindophenol (Sigma-Aldrich) at 600 nm in the presence of rotenone and KCN.[8] The enzyme assay was performed at 30 °C in a buffer containing 50 mM phosphate (pH 7.4), 0.1 μM rotenone, 2 mM KCN, 40 μM 2,6-dichlorophenolindophenol, and 12 μg ml$^{-1}$ SMP with or without napyradiomycin A1. Theonoyl trifluoroacetone (Sigma-Aldrich) was used as a positive control of complex II inhibitor.[9] We found that napyradiomycin A1 inhibited complex II activity with an $IC_{50}$ value of 9.7 μM (Figure 2b).

Mitochondrial complex III activity was measured by monitoring the absorbance change of the reduction of oxidized cytochrome *c* at 550 nm in the presence of rotenone, KCN and an electron donor decylubiquinol. Decylubiquinol was obtained by the reduction of DB with sodium borohydride.[10] The enzyme assay was performed at 30 °C in a buffer containing 50 mM Tris (pH 7.6), 1 mM $MgCl_2$, 0.1 μM rotenone, 2 mM KCN, 40 μM cytochrome *c*, 50 μM decylubiquinol and 12 μg ml$^{-1}$ SMP with or without napyradiomycin A1. Although antimycin A inhibited complex III activity, napyradiomycin A1 did not, even at 20 μM (Figure 2c)

Mitochondrial complex IV activity was measured by monitoring the absorbance change of the oxidation of reduced cytochrome *c* at 550 nm. The enzyme assay was performed at 30 °C in a buffer containing 50 mM Tris (pH 7.6), 1 mM $MgCl_2$, 0.1 μg ml$^{-1}$ antimycin A, 0.1 μM rotenone, 20 μM reduced cytochrome *c* and 12 μg ml$^{-1}$ SMP

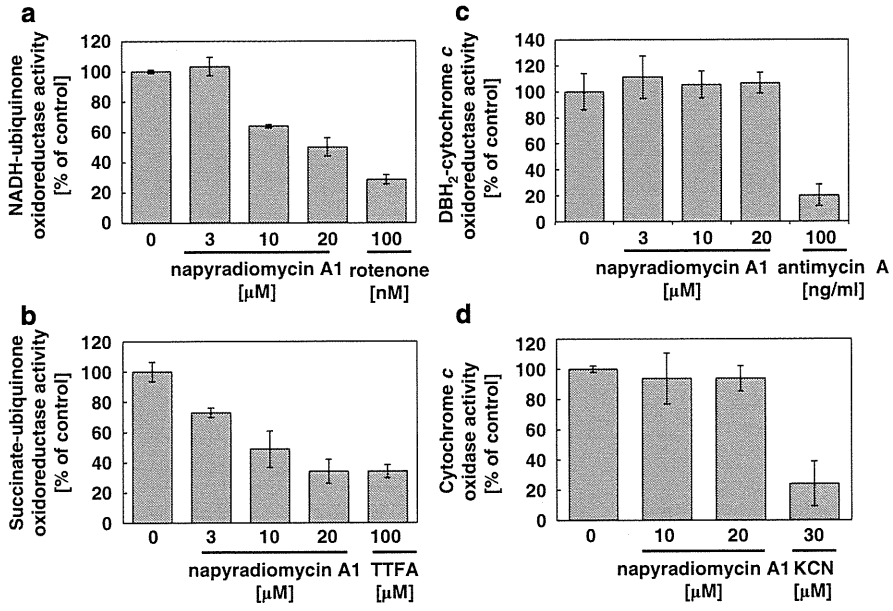


**Figure 2** Napyradiomycin A1 inhibited mitochondrial complexes I and II. A modification of previously reported methods[10,16–18] was used to measure complex I, complex II, complex III and complex IV activities. (**a**) Napyradiomycin A1 inhibited complex I activity. Mitochondrial complex I (NADH–ubiquinone oxidoreductase) activity was measured by monitoring the absorbance change of NADH at 340 nm using SMP. (**b**) Napyradiomycin A1 inhibited complex II activity. Mitochondrial complex II (Succinate–ubiquinone oxidoreductase) activity was measured by monitoring the absorbance change of 2,6-dichlorophenolindophenol at 600 nm using SMP. (**c**) Napyradiomycin A1 did not inhibit complex III activity. Mitochondrial complex III (decylubiquinol ($DBH_2$)–cytochrome *c* oxidoreductase) activity was measured by monitoring the absorbance change of cytochrome *c* at 550 nm using SMP. (**d**) Napyradiomycin A1 did not inhibit complex IV activity. Mitochondrial complex IV (cytochrome *c* oxidase) activity was measured by monitoring the absorbance change of the oxidation of reduced cytochrome *c* at 550 nm using SMP. SMP were obtained by standard different centrifugation.[4] All data are the mean ± s.d. of three independent experiments.

with or without napyradiomycin A1. Although KCN inhibited complex IV activity, 20 μM napyradiomycin A1 inhibited complex IV activity less than 10% (Figure 2d).

In conclusion, napyradiomycin A1 inhibited mitochondrial complexes I and II, but did not inhibit complex III or IV *in vitro*. Therefore, it was suggested that mitochondrial electron transport inhibition by napyradiomycin A1 was caused by the inhibition of mitochondrial complexes I and II.

It was reported that the isoprenyl unit of ubiquinone was important to bind to mitochondrial complex I.[11] It has been also reported that two isoprene units of ubiquinone could be modeled in the native structure of complex II by computational analysis using a protein-ligand docking program.[12] Napyradiomycin A1 is structurally similar to ubiquinone (Figure 1a); therefore, it is likely that napyradiomycin A1 binds with the ubiquinone-binding site of complexes I and II through its terpenoid residue. On the other hand, although mitochondrial complex III also includes a ubiquinone-binding site,[13] napyradiomycin A1 was unable to inhibit the activity of complex III up to 20 μM. Our result that napyradiomycin A1 inhibits mitochondrial complexes I and II but not complex III is interesting, because it has been reported that the structure of ubiquinone-binding sites in complex I and complex III may be similar, but they are different from a ubiquinone-binding site in complex II.[14] Further study is necessary to elucidate the mechanism by which napyradiomycin A1 inhibits mitochondrial complexes I and II but not complex III.

Isolation of napyradiomycins was first reported in 1986. Napyradiomycin group compounds were isolated from *Actinomycetes* and identified as antibacterial antibiotics.[3] At present, many napyradiomycins have been identified and reported to exhibit cytotoxicity against human cancer cell lines;[15] however, the molecular mechanism by which napyradiomycins show cytotoxicity has been unclear. Our results raise the possibility that an inhibitory effect of napyradiomycin A1 against the mitochondrial electron transport chain may explain the cytotoxicity of napyradiomycins against cancer cells.

## ACKNOWLEDGEMENTS

This study was partly supported by a Grant-in-Aid for Scientific Research from the Ministry of Education, Culture, Sports, Science and Technology of Japan. This study was also supported by grants from Suzuken Memorial Foundation. This study was supported in part by the Global COE Program for Human Metabolomic Systems Biology of MEXT, Japan.

1 Kitagawa, M., Ikeda, S., Tashiro, E., Soga, T. & Imoto, M. Metabolomic identification of the target of the filopodia protrusion inhibitor glucopiericidin A. *Chem. Biol.* **17,** 989–998 (2010).
2 Motohashi, K., Sue, M., Furihata, K., Ito, S. & Seto, H. Terpenoids Produced by Actinomycetes: Napyradiomycins from Streptomyces antimycoticus NT17. *J. Nat. Prod.* **71,** 595–601 (2008).
3 Shiomi, K. *et al.* Novel antibiotics napyradiomycins. Production, isolation, physicochemical properties and biological activity. *J. Antibiot.* **39,** 487–493 (1986).
4 Pedersen, P L. *et al.* Preparation and characterization of mitochondria and submitochondrial particles of rat liver and liver-derived tissues. *Methods Cell Biol.* **20,** 411–481 (1978).
5 di Rago, J P. & Colson, A M. Molecular basis for resistance to antimycin and diuron, Q-cycle inhibitors acting at the $Q_i$ site in the mitochondrial ubiquinol-cytochrome c reductase in *Saccharomyces cerevisiae*. *J. Biol. Chem.* **263,** 12564–12570 (1988).
6 Chance, B. The kinetics and inhibition of cytochrome components of the succinic oxidase system. III. Cytochrome b. *J. Biol. Chem.* **233,** 1223–1229 (1958).
7 Lenaz, G. *et al.* Coenzyme Q deficiency in mitochondria: kinetic saturation versus physical saturation. *Mol. Aspects Med.* **18**(Suppl), S25–31 (1997).
8 Chance, B., Williams, G R. & Hollunger, G. Inhibition of electron and energy transfer in mitochondria. I. Effects of Amytal, thiopental, rotenone, progesterone, and methylene glycol. *J. Biol. Chem.* **238,** 418–431 (1963).

9 Paddenberg, R. *et al.* Essential role of complex II of the respiratory chain in hypoxia-induced ROS generation in the pulmonary vasculature. *Am. J. Physiol. Lung Cell Mol. Physiol.* **284,** L710–719 (2003).
10 Rhein, V. *et al.* Amyloid-beta leads to impaired cellular respiration, energy production and mitochondrial electron chain complex activities in human neuroblastoma cells. *Cell Mol. Neurobiol.* **29,** 1063–1071 (2009).
11 Warncke, K. *et al.* Influence of hydrocarbon tail structure on quinone binding and electron-transfer performance at the $Q_A$ and $Q_B$ sites of the photosynthetic reaction center protein. *Biochemistry* **33,** 7830–7841 (1994).
12 Horsefield, R. *et al.* Structural and computational analysis of the quinone-binding site of complex II (succinate-ubiquinone oxidoreductase): a mechanism of electron transfer and proton conduction during ubiquinone reduction. *J. Biol. Chem.* **281,** 7309–7316 (2006).
13 Xia, D. *et al.* Crystal structure of the cytochrome $bc_1$ complex from bovine heart mitochondria. *Science* **277,** 60–66 (1997).
14 Tan, A. K., Ramsay, R. R., Singer, T. P. & Miyoshi, H. Comparison of the structures of the quinone-binding sites in beef heart mitochondria. *J. Biol. Chem.* **268,** 19328–19333 (1993).
15 Soria-Mercado, I. E., Prieto-Davo, A., Jensen, P. R. & Fenical, W. Antibiotic terpenoid chloro-dihydroquinones from a new marine actinomycete. *J. Nat. Prod.* **68,** 904–910 (2005).
16 Brusque, A. M. *et al.* Inhibition of the mitochondrial respiratory chain complex activities in rat cerebral cortex by methylmalonic acid. *Neurochem. Int.* **40,** 593–601 (2002).
17 Telford, J. E., Kilbride, S. M. & Davey, G. P. Decylubiquinone increases mitochondrial function in synaptosomes. *J. Biol. Chem.* **285,** 8639–8645 (2010).
18 Silveira, P. C., Streck, E. L. & Pinho, R. A. Evaluation of mitochondrial respiratory chain activity in wound healing by low-level laser therapy. *J. Photochem. Photobiol. B* **86,** 279–282 (2007).

THE JOURNAL OF BIOLOGICAL CHEMISTRY VOL. 286, NO. 45, pp. 39259–39268, November 11, 2011


# Involvement of 14-3-3 Proteins in the Second Epidermal Growth Factor-induced Wave of Rac1 Activation in the Process of Cell Migration*[S]

Received for publication, April 27, 2011, and in revised form, August 11, 2011 Published, JBC Papers in Press, August 25, 2011, DOI 10.1074/jbc.M111.255489

**Hiroki Kobayashi[‡], Yusuke Ogura[§], Masato Sawada[‡], Ryoji Nakayama[‡], Kei Takano[‡], Yusuke Minato[‡], Yasushi Takemoto[‡], Etsu Tashiro[‡], Hidenori Watanabe[§], and Masaya Imoto[‡1]**

*From the [‡]Department of Biosciences and Informatics, Faculty of Science and Technology, Keio University, 3-14-1 Hiyoshi, Kohoku-ku, Yokohama 223-8522, Japan and the [§]Graduate School of Agricultural and Life Sciences, The University of Tokyo, 1-1-1 Yayoi, Bunkyo-ku, Tokyo 113-8657, Japan*

**Background:** The spatiotemporal regulation of Rac1 controls cell migration.
**Results:** EGF induced two waves of Rac1 activation in the process of cell migration.
**Conclusion:** 14-3-3 proteins regulate the second EGF-induced wave of Rac1 activation by interacting with RacGEF.
**Significance:** The second wave of Rac1 activation might be required for EGF-induced cell migration.

**Immense previous efforts have elucidated the core machinery in cell migration, actin remodeling regulated by Rho family small GTPases including RhoA, Cdc42, and Rac1; however, the spatiotemporal regulation of these molecules remains largely unknown. Here, we report that EGF induces biphasic Rac1 activation in the process of cell migration, and UTKO1, a cell migration inhibitor, inhibits the second EGF-induced wave of Rac1 activation but not the first wave. To address the regulation mechanism and role of the second wave of Rac1 activation, we identified 14-3-3ζ as a target protein of UTKO1 and also showed that UTKO1 abrogated the binding of 14-3-3ζ to Tiam1 that was responsible for the second wave of Rac1 activation, suggesting that the interaction of 14-3-3ζ with Tiam1 is involved in this event. To our knowledge, this is the first report to use a chemical genetic approach to demonstrate the mechanism of temporal activation of Rac1.**

The importance of cell migration is evident from the number of physiological processes that depend on the regulated movement of cells, including embryonic development, immune responses, and tissue maintenance and repair, and also from the disease states driven by aberrant cell motility, such as chronic inflammation, vascular disease, and tumor metastasis (1). Key to the capacity of the cell to migrate is dynamic reorganization of the actin cytoskeleton (2). When a cell moves, site-directed *de novo* nucleation and polymerization of actin drives protrusive membrane structures such as lamellipodia and filopodia, which generate the locomotive force in migrating cells (3, 4). Reorganization of the actin cytoskeleton is regulated by actin-nucleating factors, the most prominent of which is the Arp2/3 complex (5). Catalytic activation of this complex is mediated by WASP/WAVE family members, which in turn translate extracellular signals via the Rho family of small GTPases such as RhoA, Cdc42, and Rac1 (6). In particular, activation of RhoA increases cell contractility and leads to the formation of focal adhesions and stress fibers (7). Activation of Cdc42 and Rac1 propagates the formation of filopodia and lamellipodia, respectively (8, 9).

The Rho family GTPases function as binary switches that cycle between an active GTP-bound form and an inactive GDP-bound form. This cycling is regulated through three factors: guanine nucleotide exchange factor (GEF),[2] GTPase-activating protein, and guanine nucleotide dissociation inhibitor (10, 11). Among them, GEF activates the Rho family GTPases by promoting the exchange of GDP with GTP, resulting in the binding of the GTPases to their effectors. A number of GEFs have been shown to transduce signals from many growth factors to the Rho family GTPases. In addition to the increasing number of GEFs, the redundant specificity of GEFs renders signaling networks controlling cell migration difficult to understand; many GEFs have been shown to take multiple Rho family GTPases as substrates, at least *in vitro* (11, 12). The spatiotemporal coordination of the Rho family GTPases by these molecules regulates a complicated dynamic process of cell migration.

Inhibitors of cell migration would be useful not only as tools for basic research into cell migration but also as anti-metastatic drug-leads for cancer therapy. To obtain cell migration inhibitor, UTKO1 was synthesized as a derivative of natural products moverastins, which inhibit migration of EC17 cells by inhibiting farnesylation of H-Ras (13). However, although its chemical structure is very similar to that of moverastins, its inhibitory effect on cell migration was stronger than that of the moverastins and did not involve inhibition of farnesyltransferase (14). UTKO1 also failed to inhibit MEK/ERK and the PI3K/Akt path-

* This work was supported by a grant from the Ministry of Education, Culture, Sports, Science, and Technology.
[S] The on-line version of this article (available at http://www.jbc.org) contains supplemental text, Scheme S1, and Figs. S1–S9.
[1] To whom correspondence should be addressed: Dept. of Biosciences and Informatics, Faculty of Science and Technology, Keio University, 3-14-1 Hiyoshi, Kohoku-ku, Yokohama 223-8522, Japan. Tel./Fax: 81-45-566-1557; E-mail: imoto@bio.keio.ac.jp.

[2] The abbreviations used are: GEF, guanine nucleotide exchange factor; IP, immunoprecipitation; CBB, Coomassie Brilliant Blue; EGF, epidermal growth factor.

way generally known to regulate cell migration.[3] This unique pharmacological profile of UTKO1 has drawn considerable interest, prompting us to further investigate its mechanism of action. In this report, we present evidence that EGF induces two waves of Rac1 activation in the process of cell migration and that UTKO1 inhibited only the second of these waves by targeting 14-3-3ζ. Furthermore, we showed that UTKO1 abrogated the binding of 14-3-3ζ to Tiam1 that was responsible for the second wave of Rac1 activation, presumably resulting in the inhibition of EGF-induced cell migration.

## EXPERIMENTAL PROCEDURES

*DNA Constructs*—Human cDNA for 14-3-3s (α/β, ε, η, γ, τ/θ, ζ/δ, and σ) were amplified from HeLa cell cDNA and cloned into pcDNA3 (Invitrogen, San Diego, CA) with the N-terminal FLAG tag. All of the constructs were cloned into pGEX-2T (GE Healthcare, Princeton, NJ) to prepare GST fusion proteins in bacteria. Expression vectors encoding GST-fused 14-3-3ζ mutants (ΔC100, 1–145 amino acids; ΔC200, 1–45 amino acids; and C50, 196–245 amino acids) were generated by PCR using pGEX-2T/14-3-3ζ as a template. pCS2+MT/Tiam1, a expression vector encoding human Tiam1 followed by 6×Myc, was kindly provided by Dr. H. Sugimura (Hamamatsu University School of Medicine, Hamamatsu, Japan).

*Chemotaxis Chamber Assay*—Cell migration was assayed with a chemotaxis chamber (Becton Dickinson, Franklin Lakes, NJ). A431 cells suspended in DMEM supplemented with 0.2% calf serum were incubated in the upper chamber; the lower chamber contained DMEM supplemented with 0.2% calf serum in the presence or absence of EGF (30 ng/ml). Drugs were added to both chambers. Following 24 h of incubation, the filter was fixed with MeOH and stained with hematoxylin (Sigma, St. Louis, MO). The cells attached to the lower side of the filter were counted.

*Confocal Laser Scanning Microscopy*—Cells were fixed with 3% paraformaldehyde for 15 min and permeabilized with 0.5% Triton X-100 in PBS for 5 min. After rinsing three times with PBS, the cells were incubated in blocking buffer (1% bovine serum albumin in PBS) for 30 min then stained with Texas Red®-X phalloidin (1:100; Molecular Probes, Eugene, OR) at room temperature for 1 h. Fluorescence images were obtained using a confocal laser scanning microscope system FV1000 (Olympus, Tokyo, Japan). Lamellipodia formation (%) means the ratio of the number of cells with lamellipodia in the total cell count.

*Detection of Active Rac1*—The cells were lysed with magnesium-containing lysis buffer (25 mM HEPES, pH 7.5, 150 mM NaCl, 1% Nonidet P-40, 0.25% sodium deoxycholate, 10% glycerol, 25 mM NaF, 10 mM $MgCl_2$, 1 mM EDTA, 1 mM $Na_3VO_4$, and a protease inhibitor mixture (Roche Applied Science)). The cell lysates were cleared by centrifugation at 15,000 × *g* for 10 min at 4 °C. Pak1 PBD-agarose (Millipore, Bedford, MA) was incubated with the lysates at 4 °C for 1 h and washed three times with magnesium-containing lysis buffer, and then active Rac1 was eluted by boiling in SDS sample buffer for 5 min. The resultant samples were subjected to Western blotting.

*Identification of B-UTKO1 Binding Proteins*—A431 cells were stimulated with EGF (30 ng/ml) for 4 h. The cells were collected and sonicated twice in immunoprecipitation (IP) buffer (50 mM HEPES, pH 7.5, 150 mM NaCl, 2.5 mM EGTA, 1 mM EDTA, 1 mM DTT, and a protease inhibitor mixture) for 10 s. The cell lysates were centrifuged at 130,000 × *g* for 1 h at 4 °C. The resulting supernatant was precleared twice with avidin beads (Pierce) for 1 h and incubated with biotin (50 nmol) or B-UTKO1ox (50 nmol) and avidin beads at 4 °C overnight. The beads were washed three times with IP buffer and once with PBS. The bound proteins were eluted with 2 mM biotin in PBS and concentrated by a centrifugal filter device (Ultracel (YM-10); Millipore). The resulting proteins were subjected to SDS-PAGE followed by Coomassie Brilliant Blue (CBB) staining (see Fig. 3*B*) or immunoblotting (see Fig. 4*A*). Following CBB staining, the bands corresponding to the UTKO1 binding proteins were excised, and the gel pieces were destained with 50% $CH_3CN$ in 50 mM $NH_4HCO_3$ solution. After removal of the supernatant, cysteine residues were reduced with DTT, carbamidomethylated with indoacetamide, and the proteins were digested with trypsin at 37 °C overnight. The tryptic peptides were recovered by sequentially adding three solvent systems containing 50% $CH_3CN$ and 1% TFA; 20% HCOOH, 25% $CH_3CN$ and 15% *i*-PrOH; and 80% $CH_3CN$. The supernatants were collected and pooled into one tube, reducing the volume *in vacuo*. The dried tryptic peptides were suspended in 2% $CH_3CN$ and 0.1% TFA and applied to the following LC-MS/MS system. Chromatographic separation was accomplished with the MAGIC 2002 HPLC system (Michrom BioResources). Peptide samples were loaded onto a Cadenza C18 custom-packed column (0.2 × 50 mm; Michrom BioResources) and eluted using a linear gradient of 5–60% $CH_3CN$ in 0.1% HCOOH for 30 min at a flow rate of 1 ml/min. Samples were ionized with a Nanoflow-LC ESI, and MS/MS spectrum data were obtained with an LCQ-Deca XP ion trap mass spectrometer (Thermo Electron). The Mascot data base searching software (Matrix Science) was used for the identification of B-UTKO1ox binding proteins.

*Immunoprecipitation*—A431/FLAG-14-3-3ζ cells were transiently transfected with pCS2+MT/Tiam1 using Metafectene Pro (Biontex, Munich, Germany). Following 24 h of transfection, the cells were pretreated with UTKO1 for 15 min and stimulated with EGF for 12 h. The cells were collected and sonicated in IP buffer. The cell lysates were cleared by centrifugation at 15,000 × *g* for 15 min at 4 °C then incubated with anti-FLAG antibody and protein A/G-agarose beads (Santa Cruz, Santa Cruz, CA) at 4 °C overnight. The immunoprecipitants were washed once with IP buffer and twice with IP buffer containing 1% Nonidet P-40. The bound proteins were eluted by boiling in SDS sample buffer for 5 min and subjected to Western blotting.

*In Vitro B-UTKO1 Pulldown Assay*—GST fusion proteins, which were expressed in the *Escherichia coli* DH5α strain and purified using glutathione-Sepharose 4B (GE Healthcare), were incubated with B-UTKO1ox and avidin beads in 500 μl of IP

[3] S. Magi and M. Imoto, unpublished observations.

buffer for 3 h. The beads were washed and eluted with 2 mM biotin in PBS. The eluted proteins were subjected to SDS-PAGE. For the competition assay, UTKO1 was added before incubating with B-UTKO1ox.

*GST Pulldown Assay*—The collected cells were sonicated twice in IP buffer for 10 s. The cell lysates were cleared by centrifugation at 15,000 × *g* for 15 min at 4 °C and then incubated with purified GST or GST-14-3-3ζ and glutathione-Sepharose 4B (GE Healthcare) for 2 h. The bound proteins were eluted by boiling in SDS sample buffer for 5 min and subjected to Western blotting. For Fig. 6*A*, purified GST-14-3-3ζ was preincubated with UTKO1 in a total volume of 1 ml of IP buffer for 1 h. Other experimental procedures are given in the supplemental materials.

## RESULTS

*UTKO1 Inhibits the Second EGF-induced Wave of Lamellipodia Formation*—The formation of lamellipodia, protruding membrane structures at the leading edge of migrating cells, is key in cell migration (15). We observed transient lamellipodia formation at 5 min following EGF stimulation, as reported elsewhere (12, 16), and we also found a second wave of lamellipodia formation to be initiated at 6–9 h and reach its zenith within 12 h after EGF stimulation in human epidermoid carcinoma A431 cells (Fig. 1, *A* and *B*). Furthermore, we found that UTKO1 (Fig. 1*C*), a cell migration inhibitor (14), inhibited only the second wave of that as shown in Fig. 1 (*D–G*); we evaluated the effect of UTKO1 on the lamellipodia formation induced by treatment with EGF for 5 min and for 12 h, respectively, and found no inhibition of lamellipodia formation at 5 min; lamellipodia formation at 12 h was inhibited by UTKO1 with an $IC_{50}$ value of 0.78 μM. This $IC_{50}$ value is almost the same as that for inhibiting cell migration (0.67 μM; Fig. 1*H*). Similar results were obtained when TT cells, a human esophageal cancer cell line, were used in place of A431 cells (supplemental Fig. S1). Thus, although EGF induced two waves of lamellipodia formation, at 5 min and 12 h after stimulation, UTKO1 inhibited only the second wave.

*UTKO1 Inhibits the Second EGF-induced Wave of Rac1 Activation*—Lamellipodia formation has been reported to be mainly regulated by Rac1, a member of the Rho family of small GTPases (9, 17). Because lamellipodia formation was observed at 5 min and 12 h following EGF stimulation, we next examined whether EGF also induces two waves of Rac1 activation. Rac1 was rapidly and transiently activated at 2–5 min after EGF stimulation, as expected from previous published reports (12, 18), and we also found that active Rac1 began to increase from 6 h onward. This second wave of Rac1 activation was much broader than the first wave and lasted until 12 h after EGF stimulation (Fig. 2*A*). UTKO1 did not inhibit the first wave of Rac1 activation even when the cells were pretreated with UTKO1 for 12 h but did inhibit the second wave (Fig. 2, *B* and *C*). Similar results were obtained when TT cells were used in place of A431 cells (supplemental Fig. S2). Moreover, when UTKO1 was added at 4 h after EGF stimulation, the second EGF-induced wave of Rac1 activation, lamellipodia formation, and cell migration were all inhibited (Fig. 2, *D–F*). These results indicate that UTKO1 suppresses EGF-induced cell migration, possibly via inhibition of the second wave of Rac1 activation required for lamellipodia formation.

*Identification of 14-3-3ζ as a UTKO1-binding Protein*—To elucidate the mechanism for the inhibition of cell migration caused by UTKO1, we tried to identify the target protein of UTKO1 responsible for Rac1 activation at 12 h following EGF stimulation. We used biotinylated UTKO1s (B-UTKO1ox and B-UTKO1ph) (Fig. 3*A* and supplemental Scheme S1), which were biologically active with the same potency as UTKO1. Lysates of A431 cells stimulated with EGF for 4 h were incubated overnight with B-UTKO1ox and avidin beads. The B-UTKO1ox-bound avidin beads were precipitated and washed, and co-precipitated proteins were eluted by excess biotin. The eluted proteins were separated by SDS-PAGE and detected by CBB staining (Fig. 3*B*). We observed 10 major protein bands that specifically co-precipitated with B-UTKO1oxand identified these proteins by LC-MS/MS system as: 1) GRP78; 2) PDI; 3) nucleobindin-2; 4) 2-phosphopruvate-hydratase α-enolase; 5) unnamed product; 6) unnamed product; 7) mutant β-actin; 8) annexin A2; 9) 14-3-3ε; and 10) 14-3-3ζ. The peptide sequences of unnamed products 5 and 6 suggest them to be nuclear lamin proteins. Of these 10 proteins, we speculated that 14-3-3ζ might be the target of UTKO1, because it has been previously reported to relate to the formation of lamellipodia (19, 20). The binding of UTKO1 to 14-3-3ζ was confirmed by Western blotting of B-UTKO1ox- or B-UTKO1ph-bound proteins using anti-14-3-3ζ antibody, as shown in Fig. 4*A*. Next, to determine whether UTKO1 could bind directly to 14-3-3ζ, we performed *in vitro* B-UTKO1 pulldown experiments using purified GST-tagged 14-3-3ζ. GST-14-3-3ζ co-precipitated with B-UTKO1ox: competition was clearly observed in the presence of UTKO1 (Fig. 4*B*). These results suggest that UTKO1 binds directly to 14-3-3ζ. Moreover, we found that B-UTKO1ox did not bind to a C terminus deletion mutant of 14-3-3ζ, indicating that the binding of UTKO1 to 14-3-3ζ is probably via the C-terminal region (supplemental Fig. S3). 14-3-3ζ is a member of the 14-3-3 family, and at least seven different isoforms have been identified in mammalian cells (21, 22). Therefore, we prepared seven recombinant GST-14-3-3 isoforms and performed *in vitro* B-UTKO1 pulldown experiments to test each for its ability to bind to UTKO1. As a result, the ζ isoform showed the strongest binding ability to B-UTKO1ox (Fig. 4*C*).

Next, we performed RNAi experiments to investigate whether the loss of 14-3-3ζ could suppress EGF-induced cell migration, lamellipodia formation, and Rac1 activation in A431 cells. The successful knockdown of 14-3-3ζ by siRNA was confirmed by Western blotting (Fig. 4*D*). Silencing of 14-3-3ζ expression consequently suppressed EGF-induced cell migration in A431 cells (Fig. 4*E*). Furthermore, silencing of 14-3-3ζ expression did not inhibit EGF-induced Rac1 activation at 2 min and lamellipodia formation at 5 min but did inhibit both EGF-induced Rac1 activation and lamellipodia formation at 12 h, as shown in Fig. 4 (*F–H*). These results indicate that 14-3-3ζ acts upstream of the second EGF-induced wave of Rac1 activation. Additionally, EGF-induced filopodia-like structures observed in 14-3-3ζ knockdown A431 cells (Fig.

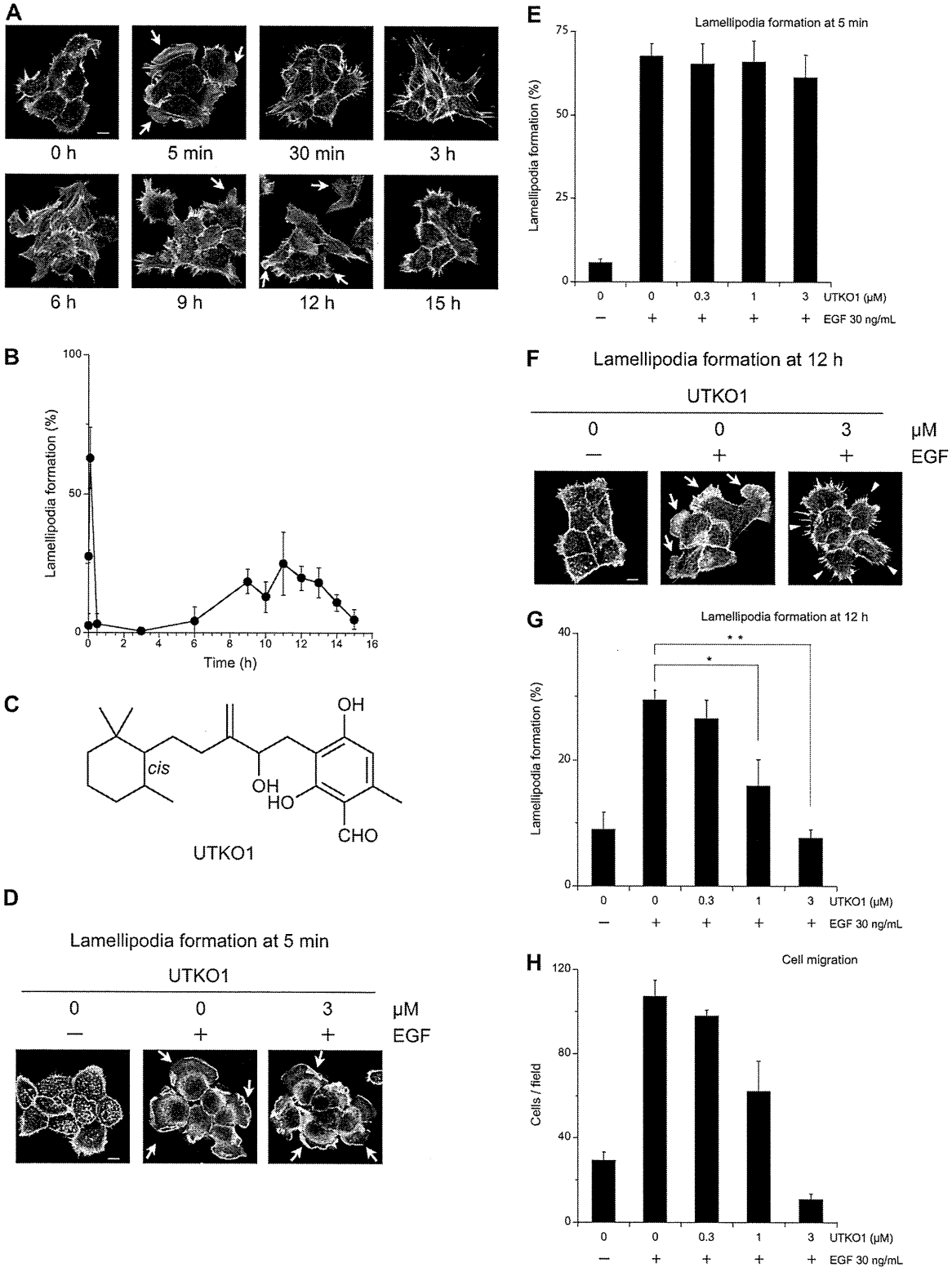


FIGURE 1. **UTKO1 inhibits the second EGF-induced wave of lamellipodia formation in A431 cells.** *A* and *B*, EGF-induced lamellipodia formation in A431 cells, observed under confocal microscopy (*A*) and counted (*B*). *C*, structure of UTKO1. *D–G*, effect of UTKO1 on EGF-induced lamellipodia formation. A431 cells were pretreated with the indicated concentrations of UTKO1 for 15 min and stimulated with EGF. After 5 min (*D* and *E*) or 12 h (*F* and *G*), the cells were observed under confocal microscopy (*D* and *F*) and counted (*E* and *G*). The data represent the means ± S.D. ($n = 6$). *H*, inhibitory activity of UTKO1 on EGF-induced cell migration, monitored using a chemotaxis chamber. The data represent the means ± S.D. ($n = 5$). Throughout, the data were representative of at least three independent studies. *Arrows*, lamellipodia; *arrowheads*, see text. *Scale bar*, 10 μm. For *G*, statistical analyses were performed with a two-tailed Student's *t* test. *, $p = 0.00013$; **, $p = 1.0 \times 10^{-5}$. For *B*, *E*, and *G*, more than 300 cells were analyzed per experiment.

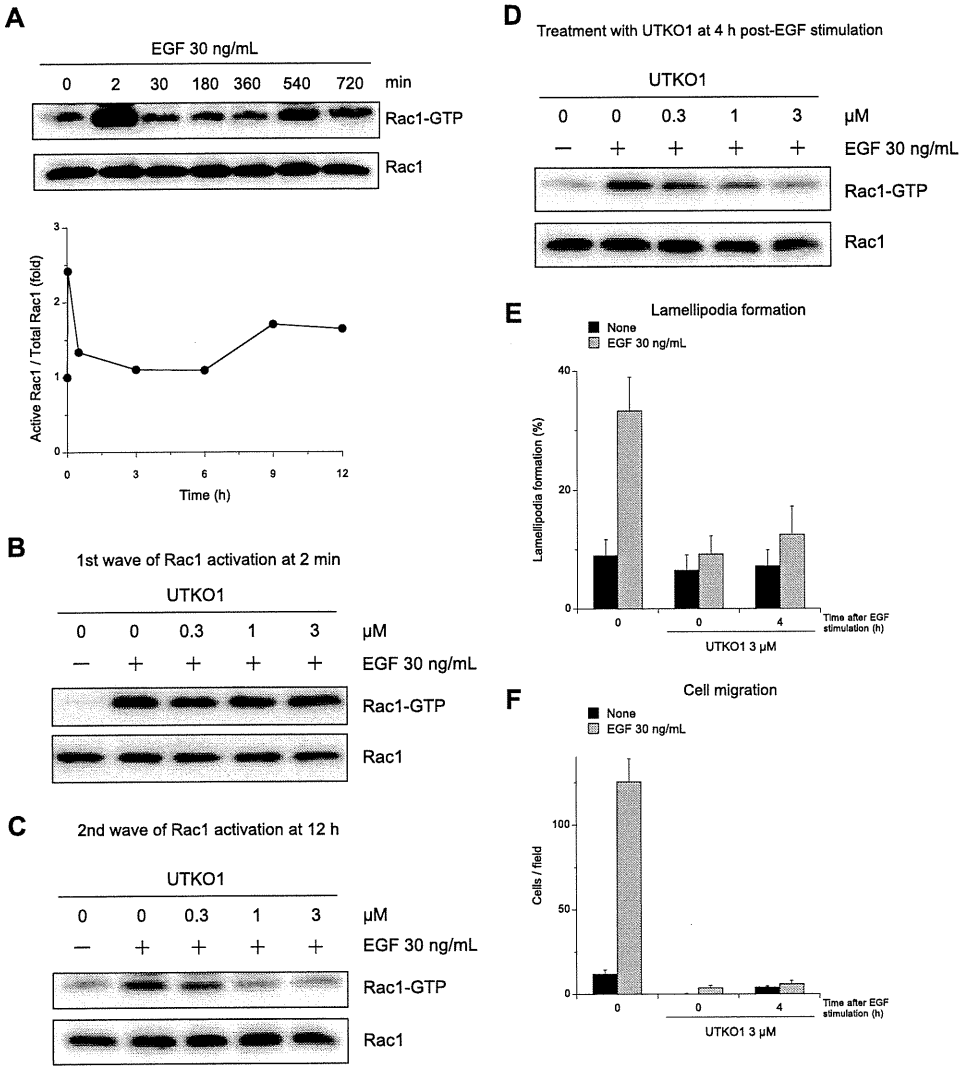


FIGURE 2. **UTKO1 inhibits the second EGF-induced wave of Rac1 activation in A431 cells.** *A*, time course analysis of Rac1 activation following EGF stimulation. A431 cells were stimulated with EGF for the indicated periods, and then the cells were examined for active Rac1 by pulldown assay (*upper panel*); signal intensities of Rac1-GTP were quantified, normalized to total Rac1 expression, using Image J software (National Institutes of Health, *lower panel*). *B* and *C*, effect of UTKO1 on EGF-induced Rac1 activation. A431 cells were pretreated with UTKO1 for 12 h (*B*) or 15 min (*C*) and stimulated with EGF. Following 2 min (*B*) or 12 h (*C*) of incubation, the cells were examined for active Rac1 by pulldown assay. *D–F*, UTKO1 inhibits only the second wave of Rac1 activation. A431 cells were stimulated with EGF for 4 h, and then the cells were treated with 3 $\mu$M UTKO1. After a further 8 h of incubation, the cells were examined for active Rac1 by pulldown assay (*D*), or the cells with lamellipodia were counted (*E*). The data represent the means ± S.D. ($n = 6$). *F*, A431 cells were incubated in the upper chamber and stimulated with EGF. Following 4 h of incubation, the cells were treated with UTKO1. After a further 20 h of incubation, the migrated cells were counted. The data represent the means ± S.D. ($n = 5$). Throughout, the data were representative of at least three independent studies. For *E*, more than 300 cells were analyzed per experiment.

4*G*, *arrowheads*) are similar to those observed in UTKO1-treated A431 cells stimulated with EGF (Fig. 1*F*, *arrowheads*). These filopodia-like structures might be formed as the result of a failure in the formation of a branched actin network as observed in a previously reported case (23). These observations also support the conclusion that the functional defect in 14-3-3ζ was induced by the treatment of cells with UTKO1. Furthermore, we showed that UTKO1 did not affect the expression levels of 14-3-3ζ (Fig. 4*I*). Taken together, these results suggest that UTKO1 binds to and inactivates 14-3-3ζ, resulting in inhibition of the second EGF-induced wave of Rac1 activation and subsequent suppression of lamellipodia formation and cell migration.

*UTKO1 Inhibits the Interaction between 14-3-3ζ and Tiam1*—Next, we examined the mechanism underlying the inhibition of Rac1 activation caused by the binding of UTKO1 to 14-3-3ζ. First, we examined the role of 14-3-3ζ in EGF-induced Rac1 activation. Because 14-3-3 proteins act as adaptor or "chaperone molecules" and interact with various cellular proteins (24), we hypothesized that a binding partner of 14-3-3ζ would regulate the second EGF-induced wave of Rac1 activation, and the most likely candidate binding partner is RacGEF. Thus, we investigated RacGEFs to see which would interact with 14-3-3ζ at 12 h following EGF stimulation by pulldown experiments using GST-14-3-3ζ. As shown in Fig. 5*A*, we verified that 14-3-3ζ interacts with both Tiam1 and βPix, as described in previous reports (19, 25, 26). We subsequently performed RNAi experiments to examine whether these GEFs are actually responsible for the second EGF-induced wave of Rac1 activation. As shown in Fig. 5*B*,